coatings

MDPI

Review

Recent Progress in Perovskite Solar Cells: Status and Future

Ying Chen [1,2,*], Man Zhang [3], Fuqiang Li [1,2] and Zhenyuan Yang [1,2]

[1] Hubei Engineering Technology Research Center of Energy Photoelectric Device and System, Hubei University of Technology, Wuhan 430068, China
[2] School of Science, Hubei University of Technology, Wuhan 430068, China
[3] School of Electrical and Electronic Engineering, Hubei University of Technology, Wuhan 430068, China
* Correspondence: chenyddc@163.com

Abstract: The power conversion efficiency (PCE) of perovskite solar cells (PSCs) has seen effective performance upgrades, showing remarkable academic research and commercial application value. Compared with commercial silicon cells, the PCE gap is narrowing. However, the stability, cost, and large-scale production are still far behind. For scale-up preparing high-efficiency and stable PSCs, there is a variety of related research from each functional layer of perovskite solar cells. This review systematically summarizes the recent research on the functional layers, including the electron transport layer, perovskite layer, hole transport layer, and electrode. The common ETL materials, such as TiO_2, SnO_2, and ZnO, need doping and a bi-layer ETL to promote their property. Large-scale and low-cost production of perovskite layers with excellent performance and stability has always been the focus. The expensive and instability problems of Spiro-OMeTAD and electrode materials remain to be solved. The main problems and future development direction of them are also discussed.

Keywords: perovskite solar cells; electron transport layer; perovskite preparation; hole transport layer; electrode; power conversion efficiency

Citation: Chen, Y.; Zhang, M.; Li, F.; Yang, Z. Recent Progress in Perovskite Solar Cells: Status and Future. *Coatings* **2023**, *13*, 644. https://doi.org/10.3390/coatings13030644

Academic Editor: Sangmo Kim

Received: 18 February 2023
Revised: 10 March 2023
Accepted: 14 March 2023
Published: 18 March 2023

1. Introduction

The serious consumption of energy and environmental problems have aroused people's attention to renewable energy. Over the past decade, solar energy systems have proved to be the most compelling of all renewable energy systems [1]. Perovskite is considered a hopeful photovoltaic candidate due to its high optical absorption coefficient, tunable band gaps, long charge carrier life, low cost, and simple preparation process [2–7]. The power conversion efficiency (PCE) of perovskite solar cells (PSCs) has jumped from 3.8% to 25.73% (certified) [8]. As shown in Figure 1, ABX_3 is the general formula crystal structure of perovskite materials. A is a large radius cation such as $CH_3NH_3^+$ (MA^+), $NH_2CH{=}NH_2^+$ (FA^+), Cs^+, Ca^{2+}, and Sr^{2+} B is Pb^{2+}, Sn^{2+}, Ti^{4+}, Nb^{5+}, Mn^{4+}, and other small radius cations. X are anions such as O_2, F^-, Cl^-, Br^-, and I^- [9,10]. The tolerance factor t could be used to calculate the perovskite crystal structure stability. The $t = (R_A + R_X)/\sqrt{2}(R_B + R_X)$, where R_A, R_B, and R_X refer to the ionic radii of A, B, and X site ions, separately. In general, the tolerance factor of structurally stable, highly symmetrical cubic structured perovskites usually ranges from 0.813 to 1.107 [11,12]. Within this range of tolerance factors, different stabilities and band structures of perovskite materials were obtained by doping or replacing the A, B, and X site ions [13]. For example, adding Sn to Pb-based perovskites could reduce the band gap and effectively broaden the absorption spectrum in the near-infrared [14,15]. With this advantage, perovskite materials can be combined with different forbidden bandwidths of light-absorbing materials, such as Si and quantum dots, to make stacked cells, such as perovskite-Si [16,17], perovskite-chalcogenides [18,19], and perovskite-quantum dots [20].

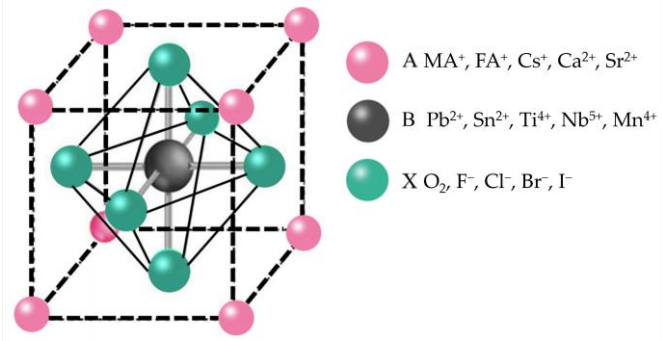

Figure 1. Typical crystalline structure of perovskite.

Perovskite solar cells are primarily divided into mesoporous structures and planar structures. The planar structures contain regular planar structures (n-i-p) and inverted planar structures (p-i-n) [21]. The typical mesoporous structures from bottom to top are a transparent conductive glass substrate (FTO, ITO), an electron transport layer (ETL), a mesoporous layer (mainly TiO_2, Al_2O_3, etc.), a perovskite layer, a hole transport layer (HTL), and metal electrodes (Figure 2a). The ETL plays the role of electron transport and hole blocking. The mesoporous layer is relatively thin. Thus, a perovskite layer could cover it completely to isolate the mesoporous material from HTL [22]. The HTL plays the role of hole transport. This structure avoids interfacial compounding of charges while maximizing charge transfer efficiency, enhancing the open-circuit voltage and charge collection efficiency, and most of the higher-certified efficiency perovskite solar cells use this structure [23]. However, the preparation of the mesoporous layers requires high-temperature processing, which limits its application in flexible devices.

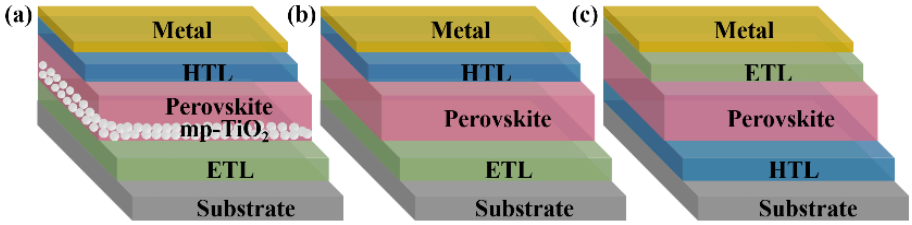

Figure 2. Three representative structures of PSCs: (**a**) mesoporous structures; (**b**) regular planar (n-i-p) structures, and (**c**) inverted planar (p-i-n) structures.

The planar structure is similar to a "sandwich structure". The perovskite layer is placed between the n-type material and the p-type material, which benefits from the excellent bipolar carrier transport properties of perovskite materials. They have n-i-p and p-i-n types (Figure 2b,c). The n-i-p structure is simplified from the mesoporous structure. The p-i-n structure is developed mainly from the structure and materials of classical organic solar cells. Planar-structured perovskite solar cells do not have a mesoporous layer, which is suitable for the fabrication of large-area flexible devices at low temperatures. Their preparation process is relatively simple too. However, without mesoporous material as a backbone, the perovskite morphology is difficult to control, the repeatability of the devices is poor, and additional auxiliary means are required to improve the film quality.

The key point of PSCs is the generation, separation, and transportation of photogenerated electrons and holes [23]. Rational selection and preparation of the functional layers are the main research priorities in this field, which is crucial for improving performance and reducing costs. In this review, we summarize the recent research status and existing problems of ETLs, perovskite layers, HTLs, and electrodes. Then, the challenges of PSCs and the strategies for improving performance are discussed.

2. Electron Transport Layer (ETL)

The ETL acts as a function of collecting electrons and blocking the transport of holes to the FTO electrode in the PSC. The mesoporous structure of the ETL promotes the crystallization and film formation of perovskite and shortens the migration path of photogenerated electrons. A suitable ETL should have an energy band position that matches the perovskite material. The conduction band position should be slightly below the conduction band minimum of the perovskite layer to facilitate electron injection, while the valence band is at a deeper position to effectively block holes and has a high electron conductivity to ensure electron transport and collection [24].

TiO_2, an N-type oxide, is considered the most common choice for ETL material, with a wide band gap (~3 eV), easy-to-tune electronic properties, ability to form both dense and mesoporous layers, and producible easily and at low cost. TiO_2 has two thermodynamically stable crystal phases: anatase and rutile. Kim et al. [25] found that the anatase phase showed better performance than the rutile phase. However, Wang et al. [26] showed that a rutile TiO_2 ETL had better conductivity and match with the $MAPbI_3$ layer, which significantly enhanced performance. Several new methods to prepare TiO_2 for flexible devices or mass production have emerged in recent years, such as ball milling [27], ultrasonic spray [28,29], atomic layer deposition [30], inkjet-print [31–33], hydrothermal [34–36], sol–gel chemistry [37], low-temperature CO_2 plasma [38], and low-temperature microwave [39,40]. The morphology of TiO_2 has also attracted much attention. $TiCl_4$ was a good choice. Jarwal et al. [41] obtained TiO_2 nanorod arrays by solvothermal etching and/or $TiCl_4$ treatment to improve their surface-to-volume ratio and direct carrier transportation. Shahvaranfard et al. [42] adopted $TiCl_4$ treatment and a $PC_{61}BM$ monolayer to obtain a TiO_2 nanorod array ETL. Lu et al. [43] exquisitely tuned $TiCl_4$ precursor solution to construct nanowire arrays and nanoflower composite of TiO_2 film. The composite structure has the characteristics of a short direct charge transmission path, small leakage current and charge transmission resistance, slow recombination rate, and large light harvest. The best PCE was more than 20%. Doping is a great method for improving the quality of TiO_2. The commonly doped materials include Li [44], Mg [45], Zn [46,47], $EuAc_3$ [48], Nb [49], Ce [50,51], Zr [52,53], Ta [54,55], and graphene quantum dots (QDs) [56]. The performance of related PSCs is shown in Table 1. Bilayer ETLs also work well, such as TiO_2/SnO_2 [57–66], TiO_2/ZnO [67,68], TiO_2/WO_3 [69,70], TiO_2/graphene [71,72], TiO_2/fullerene [73], and TiO_2/NiO [74].

SnO_2, as an ETL material, has excellent electrical and optical properties. Its disadvantage is that there are surface defects and hysteresis phenomena. Cao et al. [75] used pyrrolidine fullerene C_{60}-substituted phenol (NPC_{60}-OH) to weaken the hysteresis of SnO_2. The SnO_2/NPC_{60}-OH-based PSCs obtained a PCE of 21.39%. Liang et al. [76] passivated SnO_2 with chlorine to improve electron mobility. The open-circuit voltage increased from 1.195 V to 1.135 V. Jiang et al. [77] adopted phosphoric acid to increase the electron collection efficiency of SnO_2 by excluding its surface dangling bonds. Wang et al. [78] passivated SnO_2 ETLs by fullerene to improve the PCE and reproducibility. Cao et al. [79] modified the SnO_2 ETL by sulfur-doped graphite carbon nitride nanosheets to obtain a PCE of 20.33%. Liu et al. [80] introduced nontoxic phytic acid (PA) into the SnO_2 to obtain the ETL with fewer defects. PA-SnO_2-based PSCs had a high PCE of 21.43%. Lin et al. [81] obtained PCE of 21.87% with a SnO_2 ETL by precursor engineering. Li et al. [82] utilized vacuum-assisted annealing to synthesize a SnO_2 ETL at 100 °C for flexible solar cells, with a PCE of 20.14%. Liu et al. [83] adopted polydentate phytic acid dipotassium (PAD) to passivate the defects of the SnO_2/perovskite interface and obtained a PCE of 19.52%. Xu et al. introduced functional polymers such as polyethylene oxide-polypropylene oxide-polyethylene oxide (P123) [84] and poly(amidoamine) (PM) [85] in SnO_2 precursor to construct a uniform and dense SnO_2 ETL. The PM-treated PSC had a PCE of up to 22.93%, with negligible hysteresis. Zong et al. used continuous spin coating to fabricate SnO_2@K:Cs [86] and SnO_2@Na:Cs ETLs [87], respectively. The better PCE was 22.06%, based on a SnO_2@Na:Cs ETL. Gu et al. [88] added NaCl to raise the charge exchange between the SnO_2 ETL and perovskite and obtained a

PCE of 21.2%. Large-scale fabrication methods include vacuum thermal evaporation [89], magnetron sputtering [90], radio frequency [91,92], sputtering deposition [93], spray deposition [94,95], atomic layer deposition [96], hydrothermal [97], and printing [98]. Doping can improve the properties of SnO_2. Common doping materials include Ga [99,100], Ta [101], Nb [102,103], Zn [104], Li [105], Zr/F [106], KF [107], Cl [108], NH_4Cl [109], and graphene quantum dots [110]. The performance of related PSCs is shown in Table 1. Double ELT is also a valid way to promote the performance of SnO_2, such as SnO_2/CdS [111], SnO_2-Ti_3C_2 Mxene [112], SnO_2/ZnO [113–115], SnO_2/TiO_2 [116,117], SnO_2/carbon nanotubes [118], SnO_2/KCl [119], SnO_2-assisted CdS [120], and NH_2-ZnO@SnO_2 [121].

ZnO, as another ETL material, has relatively large electron mobility, good light transmittance, proper work function, stability, low cost, and low-temperature preparation. Environmental friendliness, low-temperature, and large area are still hot topics of preparation method research. Zhang et al. [122] promoted the energy-level alignment and charge carrier extraction of ZnO by the sol–gel method. They also deposited ZnO by a simple water-based processing route [123]. Zhao et al. [124] used magnetron sputtering to prepare big-size grains, low defect state density, and a great optical ZnO ETL. They found that the PSCs based on an Ar/O_2 ratio of 1:4 treated ZnO had a maximum PCE of 17.22%. However, ZnO shows less chemical compatibility with the perovskite layer. Surface passivation and ion doping are frequently used strategies. Yang et al. [125] optimized the hydrophilicity of the ZnO surface with three amino compounds. They found that the PSCs with isobutylamine (IBA) modification exhibited improved stability, and PCE can reach 18.84%. Eswaramoorthy et al. [126] used plasmonic nanoparticles to modify ZnO for high PCE and stability. Commonly used doping materials are Al [127], Co [128], Mg [129,130], reduced graphene oxide (rGO) sheet/Ag [131], and PbS [132]. The performance of related PSCs is shown in Table 1.

Table 1. Summary of various PSCs performances using doped ETL.

ETL		Device Configuration	J_{sc} (mA cm^{-2})	V_{OC} (V)	FF	PCE (%)	Ref.
TiO_2	Li	FTO/c-TiO_2/Li-m-TiO_2/$MAPbI_3$/Spiro-OMeTAD/Au	22.86	1.101	0.699	17.59	[44]
	Mg	FTO/Mg-TiO_2/Perovskite/Spiro-OMeTAD/Au	22.27	1.08	0.609	14.65	[45]
	Zn	FTO/Zn-TiO_2/$MAPbI_3$/Spiro-OMeTAD/Au	21.83	1.10	0.734	17.60	[46]
	Zn	FTO/Zn-TiO_2 NAs/$(FAPbI_3)_{0.87}(MAPbBr_3)_{0.13}$/CuSCN/Carbon	22.25	0.956	0.679	14.45	[47]
	$EuAc_3$	FTO/$EuAc_3$-c-TiO_2/$CsPbI_3$/P3HT/Au	21.20	1.1	0.77	17.92	[48]
	Nb	FTO/Nb-TiO_2/$FA_{0.79}MA_{0.16}Cs_{0.05}Pb(Br_XI_{1-X})_3$/Spiro-OMeTAD/Au	24.70	1.12	0.78	21.30	[49]
	Ce	FTO/Ce-TiO_2/$MAPbI_3$/Spiro-OMeTAD/Ag	21.95	1.07	0.69	16.18	[51]
	Zr	FTO/Zr-TiO_2/$MAPbI_3$/Spiro-OMeTAD/Ag	23.66	0.92	0.567	12.35	[52]
	Zr	FTO/Zr-TiO_2/$MAPbI_3$/Spiro-OMeTAD/Au	23.57	1.076	0.716	18.16	[53]
	Ta	FTO/Ta-TiO_2/$Cs_{0.1}(FA_{0.83}MA_{0.17})_{0.9}Pb(I_{0.83}Br_{0.17})_3$/Spiro-OMeTAD/Ag	22.45	1.13	0.77	19.62	[54]
	GQDs	FTO/c-TiO_2/GQDs-mTiO_2/$Cs_{0.05}(FA_{0.83}MA_{0.17})_{0.95}Pb(I_{0.83}Br_{0.17})_3$/Spiro-OMeTAD/Au	21.92	0.97	0.63	14.36	[56]
	Ga	ITO/Ga-SnO_2/$(FAPbI_3)_x(MAPbBr_3)_{1-x}$/Spiro-OMeTAD/Ag	23.90	1.068	0.714	18.18	[99]
	Ga	FTO/Ga-SnO_x/$CsPbBr_3$/Carbon	7.58	1.311	0.602	5.98	[100]
	Ta	ITO/Ta-SnO_2/Perovskite/Spiro-OMeTAD/Au	22.79	1.161	0.786	20.8	[101]
	Nb	FTO/Nb-SnO_2/$CsPbBr_3$/Carbon	8.92	1.31	0.731	8.54	[103]
	Zn	FTO/Zn-SnO_2/$CsPbBr_3$/CuPc/Carbon	23.40	1.098	0.692	17.78	[104]

Table 1. *Cont.*

ETL		Device Configuration	J_{sc} (mA cm^{-2})	V_{OC} (V)	FF	PCE (%)	Ref.
SnO_2	Li	Li-FTO/SnO_2/Al_2O_3/$MAPbI_3$/Carbon	22.18	0.76	0.59	10.01	[105]
	Zr/F	FTO/Zr/F-SnO_2/Perovskite/Spiro-OMeTAD/Au	24.39	1.105	0.712	19.19	[106]
	KF	ITO/KF-SnO_2/$CsPbI_2Br$/ Spiro-OMeTAD/MoO_3/Au	14.79	1.31	0.792	15.39	[107]
	Cl	FTO/Cl-SnO_2/Perovskite/Spiro-OMeTAD/Au	24.25	1.07	0.73	18.94	[108]
	NH_4Cl	ITO/NH_4Cl-L-SnO_2/NH_4Cl-H-SnO_2/ Perovskite/PEAI/Spiro-OMeTAD/Au	23.60	1.208	0.762	21.75	[109]
	GQDs	ITO/GQDs-SnO_2/$MAFAPbI_3Cl_{3-x}$/ Spiro-OMeTAD/Ag	24.40	1.11	0.78	21.10	[110]
ZnO	Co	PET/ITO/Co-ZnO/$MAPbI_3$/Spiro-OMeTAD/Au	14.30	1.04	0.47	7.00	[128]
	Mg	FTO/Mg-ZnO/$MAPbI_3$/Spiro-OMeTAD/Ag	25.06	0.83	0.65	13.52	[130]
	rGO/Ag	FTO/rGO/Ag-ZnO/$MAPbI_3$/Spiro-OMeTAD/Au	17.82	0.90	0.72	11.03	[131]
	PbS	ITO/PbS-ZnO/$MAPbI_3$/Spiro-OMeTAD/Ag	22.8	1.14	0.79	20.53	[132]

3. Perovskite Layer

The property of the perovskite layer, such as thickness, grain size, grain boundary defects, and surface roughness, affects the capability of the perovskite solar directly. Various preparation methods have been developed to produce higher-quality perovskite films for high PCE and stability [133]. The main preparation methods for the perovskite layer are spin coating [134], blade coating [135], vapor deposition [136], spray coating [137,138], drop casting [139–141], dip coating [142–144], electrodeposition [145,146], screen printing [147], inkjet printing [148,149]. All the above processes have their limitations and commercial viabilities. To compete with commercial silicon cells, stability and large-scale production are the focus of research. The trend of spin coating and blade coating is towards environmentally friendly solutions. The vapor deposition is mainly on a lab scale. They have advantages in cost, design freedom, optimal use of materials, and scalability, but they still need a rapid transformation from small, laboratory-scale work to large, industrial-scale production. Some of the new mass-production methods, such as spray coating, electrodeposition, screen printing, and inkjet printing, also need to be improved in terms of efficiency and repeatability.

3.1. Spin Coating

Spin coating is the most general method to prepare low-cost and high-efficiency PSCs. It contains "one-step coating" and "two-step coating". In one-step spin coating, appropriate proportions of BX_2 (B = Pb^{2+}, Sn^{2+}, etc.) and AX (A = MA^+, FA^+, Cs^+, etc.; X = I^-, Br^-, Cl^-, etc.) are dissolved in solvents to form precursor solution, and then the precursor solution is spin-coated on the ETL with adding anti-solvent. Solvents, anti-solvent, and the annealing process are the three main points to improve the quality of perovskite. Commonly used solvents are highly toxic and environmentally hazardous, such as *N*,*N*-dimethylformamide (DMF), dimethyl sulfoxide (DMSO), *N*-methyl-2-pyrrolidone (NMP), and γ-butyrolactone (GBL) [134]. Giuliano et al. [150] employed a green solvent additive, alpha-terpineol, to promote the quality of $CH_3NH_3PbI_{3-x}Cl_x$ films. The planar n-i-p PSCs showed a PCE of 17.5% with decreased hysteresis and reinforced ambient stability. Kadhim et al. [151] obtained a high-quality Cs(MAFA)Pb$(IBr)_3$) film by using a green EA solvent. A PCE of 18.63% and a fill factor of 79.78% were obtained. Cao et al. [152] proposed a green triethyl phosphate (TEP) solvent for perovskite precursor solution, and a non-polar dibutyl ether (DBE) solvent to be anti-solvent. Then, they obtained the best PCE of 20.13%. Zhu et al. [153] used $Pb(SCN)_2$ to restrain the formation of an unacceptable PbI_2·xDMSO-H_2O compound for perfect perovskite crystallizes, and used PEASCN to increase moisture tolerance of perovskite films. $MAPbI_3$ and $MA_{0.6}FA_{0.4}PbI_3$ layers were successfully prepared in high-humidity air, and the PSCs based on them had PCEs of 19.83%

and 21.18%, respectively. Taylor et al. [154] studied the influence of antisolvent on the quality of perovskite, as shown in Figure 3. They identified that the solubility of the organic precursors in the antisolvent and its miscibility with the host solvent(s) of the perovskite precursor solution combined to influence the quality of the perovskite layer. Sin et al. [155] found that the quality of $MAPbI_3$ depended on the anti-solvent treatment (AST) time, amount, and temperature. If AST time was 9.5 s at 25 °C, the PSCs had the best PCE of 18.9%. The annealing is a necessary and critical process which serves to vaporize the solvent and induce the crystallization of perovskite [156]. Xu et al. [157] used millisecond light pulses to anneal for the crystallization of $MAPbI_3$ and fabricated PSCs rapidly, which was a hopeful method for large-area, high-performance PSC fabricating. Chen et al. [158] adopted a rapid microwave-annealing method to avoid miscellaneous phases. Serafini et al. [159] proposed that flash infrared annealing could promote the optoelectrical property of the perovskite. Turgut et al. [160] proposed a light-assisted annealing (LA) method to form larger and uniform grains of the perovskite layer.

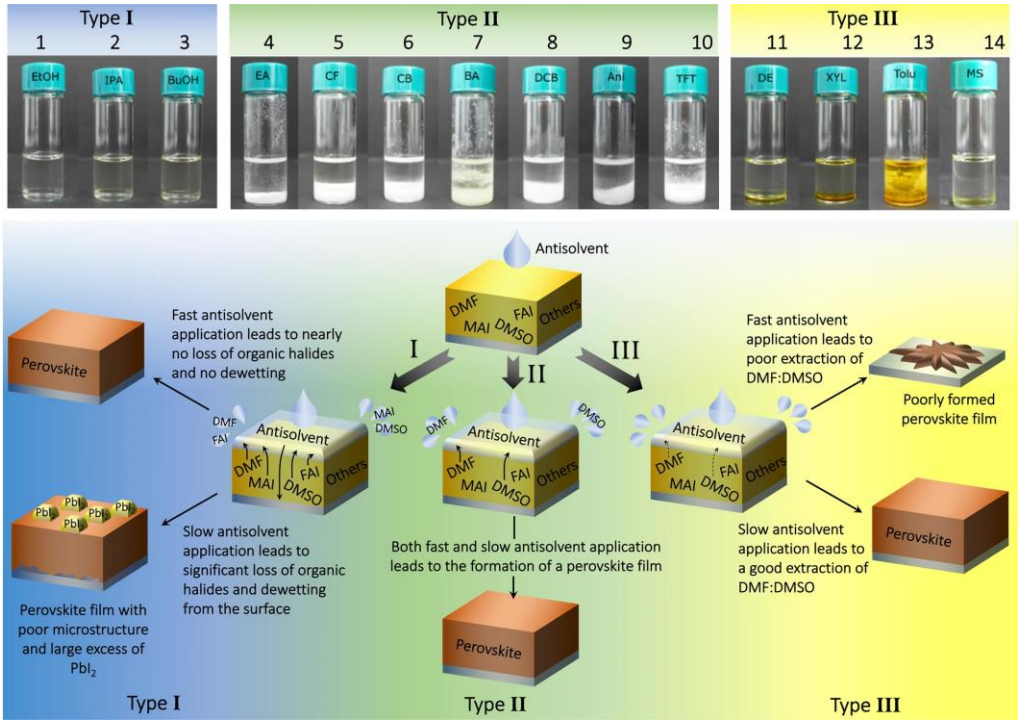

Figure 3. Summary of the processes taking place during perovskite film formation for the three antisolvent types. Top: solubility of MAI in a solution of DMF:DMSO:antisolvent, meant to simulate the perovskite film intermediate phase during the antisolvent step of fabrication. Bottom: summary of the various mechanisms involved in perovskite film formation by the different categories of antisolvents [154].

Overall, the advantage of one-step spin coating is the utilization of solution processing in the production of the perovskite layer, which simplifies the production process and reduces costs. However, there are many limitations in the production of perovskite films and stringent testing conditions, which places high demands on the actual conditions and processes used to produce the films.

Two-step spin coating involves spin coating BX_2 on the substrate to form BX_2 film, then spin coating AX on it to form a perovskite layer. This method could obtain fine perovskite morphology with great reproducibility. The disadvantage is that excess PbI_2 can affect the performance of the final perovskite. Therefore, some recent research focuses on converting excess PbI_2 into perovskite. Li et al. [161] used the remaining dimethyl sulfoxide (DMSO) to adjust the crystallization of PbI_2. They also tried to delay the crys-

tallization of PbI_2 by adding dithizone into the PbI_2 precursor [162]. Luan et al. [163] adjusted the concentration of organic salts in the precursor solution for the second step to translate all PbI_2 to perovskite successfully. Both the PCE (21.26%) and stability of the PSCs without excessive PbI_2 have been significantly improved. Jiao et al. [164] replaced PbI_2 with $FA_4Pb_3I_6Ac_4$ (Ac^-: CH_3COO^-) to fabricate stable black-phase $FAPbI_3$ and obtain a PCE of 23.65% with high reproductivity, due to avoiding the extra PbI_2. Bi et al. [165] fabricated high-phase purity and large grains of the $CsPbBr_3$ perovskite layer by a facile thiourea-assisted two-step spin-coating method. In the first step, thiourea was added into the $PbBr_2$ layer to improve its wettability. In the second step, green high-concentration $CsBr/H_2O$ solution provided enough CsBr to deposit. Thus, the $CsPbBr_3$ PSC with a carbon electrode obtained a high PCE of 9.11%. The unencapsulated device showed fine stability. Zhi et al. [166] added N-methyl-2-pyrrolidone (NMP) in the MAI/IPA solution, then annealed in closed steam to intensify the Oswald ripening effect for the high-quality $CH_3NH_3PbI_3$ layer. In addition, the low solubility of Cs salts is a problem for perovskite quality. Cheng et al. [167] used ethanol and methanol mixed solvent to improve the solubility of CsI and obtained a high-quality $FA_{1-x}Cs_xPbI_3$.

Chang et al. [168] found that the one-step spin coating obtained more MA^+, resulting in a P-type majority carrier-type perovskite layer. The two-step spin coating obtained more Pb^{2+}, resulting in an N-type majority carrier-type perovskite layer. The one-step spin coating had extra PbI_2, which was harmful to the interface and the perovskite layer quality. Liu et al. [169] studied the difference between one-step spin coating and two-step spin coating from crystalline growth mode, optical properties, defect types, and carrier transport mechanisms. They found that the two-step spin coating obtained a smaller open-circuit voltage and fill factor, but a bigger short-circuit current.

3.2. Blade Coating

Blade coating has some obvious advantages, such as large-area preparation, high PCE, easy manipulation, and low cost, and includes doctor-blade coating, slot-die coating, and roller coating. Substrate temperature, blade coating speed, and precursor concentration are important factors of blade coating [135]. The most processing challenge was ambient moisture [170]. Wang et al. [171] ensured the perovskite phase transition by the appropriate substrate temperature and delayed perovskite crystallization by the dimethyl sulfoxide (DMSO) in the precursor solution. Thus, the doctor-blade coating prepared a large-grained perovskite layer, helping the PCE to 15.34%. Lee et al. [172] used the optimum substrate temperature and appropriate solvent ratio to n-i-p and p-i-n PSCs. The PCEs were 17.55% and 16.90%. Yu et al. [173] found that butyltrimethylammonium chloride (BTACl) passivation could reduce the influence of ambient humidity on the blade coating process, which produced a PCE of 20.5% with negligible hysteresis. Zendehdel et al. [174] combined blade and spin coating to improve the utilization rate of precursor materials. They fabricated a 10 cm^2 active area of PSCs with an 18.8% PCE via blade-spin/blade deposition.

Vijayan et al. [175] adjusted the deposition parameters of the slot-die coating to obtain a dense and highly crystalline perovskite layer, which obtained a PCE of 14.5%. Huang et al. [176] used slot-die coating and near-infrared irradiation heating to make an area of 12 × 12 cm^2 PSCs in air rapidly. Bernard et al. [177] enhanced the perovskite quality by adding methylammonium chloride into the ink formulation, then used vacuum solvent extraction to obtain a stabilized PCE of 17.6%. Bisconti et al. [178] synthesized good morphology perovskite layer at 60 °C for flexible solar cells by starch-polymer-assisted slot-die coating. Li et al. [179] found that 12 mol% DMSO as an additive of the slot-die coating ink formulation could block the intermediate phase about $MAPbI_3$ and $MAPbI_3$-2-ME and induce $MAPbI_3$ crystallization, improving the PCE to 20.8% (Figure 4).

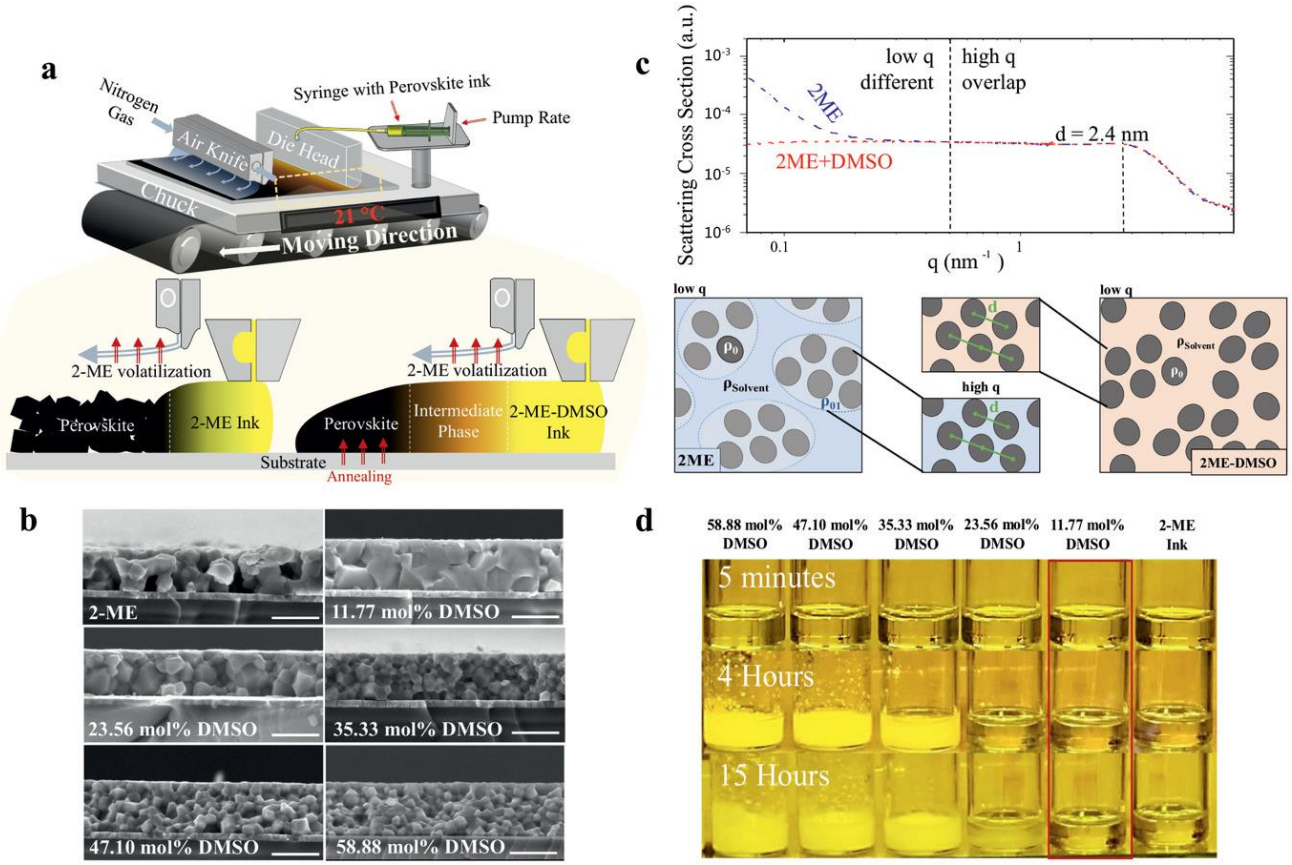

Figure 4. Schematic illustration of slot-die coating. (**a**) Coating from 2-ME and 2-ME-DMSO inks; (**b**) Cross-section SEM images (scale bar is 800 nm); (**c**) SAXS curves of two backgrounds, subtracting scattering curves of $MAPbI_3$ in 2-ME (blue) compared to MAPI in 2ME with 11.77 mol% DMSO (red). Both solutions are in the same concentration; (**d**) Images of 2-ME DMSO inks (in the duration of 1 to 15 h) stored inside the glovebox (with O_2 and H_2O levels less than 1 ppm) [179].

3.3. Vapor Deposition

Vapor deposition methods include high-vacuum deposition techniques (such as thermal evaporation) and low-vacuum deposition techniques (such as hybrid chemical vapor deposition) [136]. Vaynzof [180] compared thermal evaporation and solution processing. He reported that the difference in performance was diminishing and that thermal evaporation was more promising for commercial use. Choi et al. [181] fabricated large-area (250 mm^2) and scalable (75 × 75 mm^2) PSCs by the all-vacuum deposition method. In addition, stability is also important. There is much less research on stability improvement in thermal evaporation than the solution method [182]. Li et al. [183] used mixed-vapor deposition to prepare a $PEA_2MA_{n-1}Pb_nI_{3n}$, which improved PCE to 18.08%. Lohmann et al. [184] controlled the crystallite size of the $CH_3NH_3PbI_3$ layer by managing the substrate temperature when co-deposition of PbI_2 and organic CH_3NH_3I. Qiu et al. [185] adopted rapid hybrid chemical vapor deposition (HCVD) to prepare 22.4 cm^2 PSCs with a PCE of 12.3%. Qiu et al. [186] presented the recent development of modified CVD. They showed the potential of modified CVD for scalable fabrication of PSCs and modules with low cost. Defect passivation and interface modification are also a few relative reports. The performance of related PSCs is shown in Table 2.

Table 2. Summary of various PSC performances using various preparation methods.

Preparation Methods	Device Configuration	J_{sc} (mA cm^{-2})	V_{OC} (V)	FF	PCE (%)	Ref.
Drop casting	ITO/PEDOT:PSS/$(C_4A)_2MA_4Pb_5I_{16}$/$PC_{61}BM$/PEIE/Ag	19.18	1.12	0.702	15.08	[139]
	ITO/PEDOT:PSS/$MAPbI_3$/$PC_{61}BM$/BCP/Ag	22.76	1.08	0.756	18.57	[140]
Dip coating	FTO/TiO_2/ZnO/$MA_xFA_{1-x}PbI_3$/Spiro-OMeTAD/Ag	21.20	0.99	0.670	14.10	[142]
	FTO/TiO_2/ZnO/$MAPbI_3$/Spiro-OMeTAD/MoO_3/Ag	20.33	0.95	0.630	12.17	[143]
	FTO/TiO_2/ZnO/$MAPbI_{3-X}Cl_X$/Spiro-OMeTAD/MoO_3/Ag	21.31	1.04	0.690	15.29	[144]
Screen printing	FTO/TiO_2/Perovskite/Spiro-OMeTAD/MoO_3/Ag	23.12	1.14	0.779	20.52	[147]
Inkjet printing	ITO/PEDOT:PSS/$(BA)_2(MA)_3Pb_4I_{13}$/$PC_{61}BM$/PEIE/Ag	18.80	1.14	0.695	14.90	[148]
	FTO/TiO_2/C_{60}/$Cs_{0.05}MA_{0.14}FA_{0.81}PbI_{2.55}Br_{0.45}$/Spiro-OMeTAD/Au	23.48	1.108	0.762	19.60	[149]
Spin coating	FTO/TiO_2/$MAPbI_{3-X}Cl_X$/Spiro-OMeTAD/MoO_3/Ag	23.00	1.059	0.721	17.50	[150]
	FTO/TiO_2/$Cs(MAFA)Pb(IBr)_3$/Spiro-OMeTAD/Au	22.16	1.054	0.798	18.63	[151]
	FTO/SnO_2/$(FAPbI_3)_{0.95}(MAPbBr_3)_{0.05}$/Spiro-OMeTAD/Au	24.69	1.09	0.748	20.13	[152]
	FTO/SnO_2/$MA_{0.6}FA_{0.4}PbI_3$/PCBM/Au	23.78	1.12	0.795	21.18	[153]
	ITO/PTAA/$Cs_{0.05}FA_{0.80}MA_{0.15}PbI_{2.55}Br_{0.45}$/PCBM/$C_{60}$/BCP/Ag	23.81	1.16	0.785	21.59	[158]
	FTO/c-TiO_2/m-TiO_2/$MAPbI_3$/Spiro-OMeTAD/Au	23.90	1.08	0.75	19.50	[159]
	ITO/SnO_2/Perovskite/Spiro-OMeTAD/Au	23.60	1.14	0.771	20.66	[162]
	ITO/SnO_2/$FAPbI_3$/Spiro-OMeTAD/Ag	25.73	1.15	0.798	23.65	[164]
	FTO/TiO_2/$CsPbBr_3$/C	8.81	1.38	0.75	9.11	[165]
	FTO/TiO_2/$MAPbI_3$/Spiro-OMeTAD/Au	22.68	1.00	0.70	16.78	[166]
	FTO/SnO_2/$FA_{1-x}Cs_xPbI_3$/Spiro-OMeTAD/Ag	24.12	1.142	0.769	21.17	[167]
Blade coating	FTO/NiO_x/$MAPbI_3$/PCBM/BCP/Ag	20.93	1.113	0.688	15.34	[171]
	FTO/TiO_2/$MAPbI_3$/Spiro-OMeTAD/Ag	21.94	1.05	0.762	17.55	[172]
	FTO/c-TiO_2/m-TiO_2/3D/2D Perovskite/PTAA/Au	22.66	1.088	0.793	19.55	[174]
	FTO/c-TiO_2/m-TiO_2/$Cs_{0.17}FA_{0.83}Pb(I_{0.83}Br_{0.17})_3$/Spiro-OMeTAD/Au	20.30	1.15	0.755	17.60	[177]
	ITO/SAM/$MAPbI_3$/C_{60}/BCP/Cu	23.67	1.138	0.773	20.80	[179]
Vapor deposition	ITO/Spiro-mF/$MAPbI_3$/$PC_{61}BM$/ZnO/Ag	21.90	1.07	0.79	18.50	[181]
	ITO/PTAA/$CsPbI_3$/C_{60}/BCP/Cu	17.80	0.96	0.73	12.50	[182]
	FTO/TiO_2/C_{60}/$(PEA)_2(MA)_{n-1}Pb_nI_{3n}$/Spiro-OMeTAD/Au	23.75	1.08	0.704	18.08	[183]
	FTO/C_{60}/$MAPbI_3$/Spiro-OMeTAD/Au	21.70	1.08	0.778	18.30	[184]
	ITO/SnO_2/$Cs_{0.1}FA_{0.9}PbI_3$/Spiro-OMeTAD/Au	22.30	0.99	0.702	15.50	[185]

4. Hole Transport Layer (HTL)

The HTL is located between the perovskite layer and the counter electrode, which is very important in perovskite solar cell devices. It plays the role of fast extraction of transported photogenerated holes and blocking electrons, effectively avoiding the interface compounding caused by their direct contact. The energy level of the HTL material must coincide with the valence band maximum of the perovskite material. The difference between these two energy levels ensures hole transport, but too large an energy level difference can lead to energy loss.

The organic small molecule Spiro-OMeTAD (2,2′,7,7′-tetrakis(N,N-di-*p*-methoxyphenylamine)-9,9′-spirobifluorene) is the most common HTL material, due to its wonderful hole transport properties. However, it is expensive and unstable. Improving its stability is the key research direction [187,188]. Niu et al. [189] improved the stability of Spiro-OMeTAD by adding a hydrophobic polymeric poly(4-vinylpyridine) (P4VP). Thus, PSCs remained 80% of the original PCE (20.6%) after over 6000 h in ambient air. Zhou et al. [190] added a metal–organic framework-derived 2D graphitic N-rich porous carbon (NPC) in Spiro-OMeTAD to decrease its defects. Du et al. [191] used Sb_2S_3 nanoparticles to inhibit the Li-TFSI aggregation for a compact spiro-OMeTAD:Sb_2S_3 HTL which could block the moisture and oxygen on the perovskite layer efficiently. The PCE was 22.13%, with great chemical stability. Cao et al. [192] prepared Co(III)-grafted CN nanosheets to improve the hole extraction and reduce the interfacial recombination. PCE of the doped PSCs reached 23.01%. In addition, other useful materials have recently been reported, such as carbon quantum dots (QDs) [193], Er@C-82 [194], fluorinated Graphene [195], $PbSO_4(PbO)_4$ QDs [196], and SnS nanoparticles [197].

PEDOT:PSS (poly(3,4-ethenedioxythiophene):poly(styrene sulfonate)), as a polymer HTL material in inverted PSCs, has brilliant optical transparency. It can be prepared at low temperatures. However, low fitness of work function, conductivity, and polarity mismatch between PEDOT:PSS and perovskite materials limited its development [198]. Modification, bilayer HTLs, and doping are recently effective methods. Elbohy et al. [199] adjusted the morphology, conductivity, and work function of PEDOT:PSS with urea, improving the PCE

from 14.4% to 18.8%. Yi et al. [200] employed WO_3/PEDOT:PSS to enhance the performance of PSCs. Yang et al. [201] diluted PEDOT:PSS for a less defective state density and a more appropriate work function. Sodium citrate [202], graphene [203], and ethanolamine [204] are the doping materials reported recently.

There is more and more research about NiO as an HTL material for inverted PSCs. It could be prepared in low temperatures for large-scale and flexible devices too. Compared to organic HTL materials, it has inappreciable hysteresis effects and better stability. However, it still has problems with low conductivity and mismatched bands [205]. Doping is an effective method. Lee et al. [206] used near-infrared radiation annealed Co-doped NiO_x to reduce V_{oc} loss. Chen et al. [207] found that Rb^+-doped NiO_x showed higher conductivity and better energy-level alignment. Choi et al. [208] reported cerium and zinc co-doped, where Zn doping improved electrical conductivity and Ce doping optimized surface morphology. Some other inorganic materials also attract attention, such as Cu_2ZnSnS_4 [209], Cu_2ZnGeS_4 [210], CuSCN [211–213], and Cu-doped Ga_2O_3 (Ga_2O_3:Cu) [214]. Compared with the ETL materials, the HTL materials have less research, but they have more research space on preparation and performance. The performance of related PSCs is shown in Table 3.

Table 3. Summary of various PSCs performances using different HTLs.

HTL		Device Configuration	J_{sc} (mA cm^{-2})	V_{OC} (V)	FF	PCE (%)	Ref.
Spiro-OMeTAD	P4VP	ITO/PEDOT:PSS/Perovskite/Spiro-OMeTAD:P4VP/Au	23.49	1.129	0.787	20.84	[189]
	NPC	FTO/c-TiO_2/$Cs_{0.05}FA_{0.81}MA_{0.14}PbI_{2.55}Br0._{45}$/Spiro-OMeTAD:NPC/Au	23.51	1.06	0.76	18.51	[190]
	Sb_2S_3	ITO/SnO_2-KCl/CsFAMA/Spiro-OMeTAD:Sb_2S_3/Au	24.75	1.132	0.79	22.13	[191]
	Co(III)-CN	FTO/TiO_2/$Cs_{0.05}MA_{0.1}FA_{0.85}Pb(I_{0.97}Br_{0.03})_3$/Spiro-OMeTAD:$CoCN_2$/Au	25.43	1.138	0.795	23.01	[192]
	CQDs	FTO/SnO_2/$(FAPbI_3)_{0.95}(MAPbBr_3)_{0.05}$/CQDs/Spiro-OMeTAD/Ag	24.18	1.064	0.799	17.92	[193]
	$PbSO_4(PbO)_4$ QDs	ITO/SnO_2/CsFAMA/$PbSO_4(PbO)_4$-Spiro-OMeTAD/Au	24.80	1.142	0.80	22.66	[196]
	SnS	ITO/SnO_2/Perovskite/SnS- Spiro-OMeTAD/Au	24.01	1.17	0.807	22.59	[197]
PEDOT:PSS	Urea	ITO/PEDOT:PSS/$MAPbI_3$/PCBM/Rhodamine/Ag	22.57	1.03	0.809	18.80	[199]
	WO_3	ITO/SnO_2/$FA_{0.4}MA_{0.6}PbI_{2.8}Br_{0.2}$/$WO_3$/PEDOT:PSS/$MoO_3$/Ag	22.69	1.03	0.648	15.10	[200]
	Diluted	ITO/D-PEDOT:PSS/$MAPbI_{3-x}Cl_x$/C_{60}/BCP/Ag	20.56	1.08	0.804	17.85	[201]
	Citrate	ITO/SC-PEDOT:PSS/$MAPbI_{3-x}Cl_x$/PCBM/BCP/Ag	21.62	1.134	0.750	18.39	[202]
NiO	Co	FTO/NIR-4 Co:NiO_x/$MAPbI_3$/PCBM/PEI/Ag	20.46	1.09	0.798	17.77	[206]
	Rb	FTO/Rb-NiO_x/$MAPbI_3$/PCBM/BCP/Ag	23.35	1.133	0.824	21.80	[207]
	Zn-Ce	ITO/NiO_x:ZnCe/$MAPbI_3$/PCBM/BCP/Ag	22.30	1.03	0.63	14.47	[208]
Cu_2ZnGeS_4		FTO/SnO_2/$MAPbI_3$/Cu_2ZnGeS_4/C	23.10	1.082	0.721	18.02	[210]
CuSCN		FTO/c-TiO_2/$MAPbI_3$/CuSCN/Au	23.77	0.981	0.724	16.89	[212]
Ga_2O_3:Cu		FTO/Ga_2O_3:Cu/$Cs_{0.175}FA_{0.75}MA_{0.075}Pb(I_{0.88}Br_{0.12})_3$/PCBM/$C_{60}$/BCP/Ag	22.90	1.12	0.76	19.5	[214]

5. Electrode

PSC electrode materials need to have the appropriate work function, high electrical conductivity, and stability. It is inevitable to explore new low-cost electrode materials to replace traditional noble metal electrodes (Au and Ag) for a higher performance–price ratio [215,216]. Carbon materials are ideal candidates because they have similar functions and fine electrical conductivity to Au and can be prepared by silk-screen printing [217]. Lee et al. [218] reported that trifluoromethanesulfonic acid (TFMS) vapor doping of the free-standing carbon nanotube (CNT) sheet enabled the tuning of conductivity and work function of the CNT electrode. As shown in Figure 5, they found that PSCs based on TFMS 30 second-doped CNT obtained a champion PCE of 17.56%, with enhanced stability. Other carbon materials have been reported, such as mesoporous carbon [219], carbon nanofiber [220], graphite [221], and graphene [222].

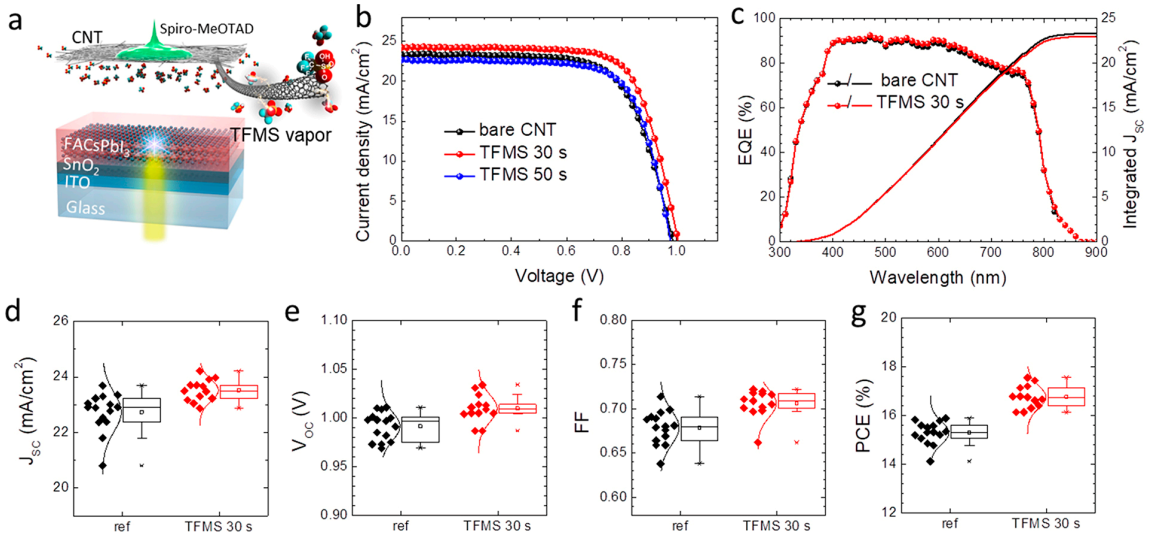

Figure 5. (**a**) Schematic illustration of planar heterojunction PSCs based on TFMS-doped CNT. (**b**) $J-V$ curves of the highest PCE PSCs, incorporating bare CNT and CNT doped by TFMS 30 and 50 s. (**c**) EQE spectra and corresponding integrated short-circuit current density (J_{SC}) of the device based on bare CNT and CNT doped by TFMS for 30 s. (**d**) J_{SC}. (**e**) open circuit voltage (V_{OC}). (**f**) fill factor (FF) and (**g**) PCE of the PSCs incorporating bare CNT and CNT doped by TFMS [218] 2019 American Chemical Society.

6. Summary

The PCE of PSCs has seen effective performance upgrades between 2009 and 2023, showing remarkable academic research and commercial application value. Compared with commercial silicon cells, the PCE gap is narrowing. However, stability, cost, and large-scale production are still far behind. We have summarized some recent research on each functional layer (ETL, perovskite layer, HTL, and electrodes) of PSCs. TiO_2, SnO_2, and ZnO are the three most commonly used ETL materials. Doping and bilayer ETLs could promote their property. The ETL, which can be obtained at low temperatures, is advantageous for application in flexible PSCs. The perovskite layer is the soul of PSCs. Large-scale and low-cost production of perovskite layers with excellent performance and stability has always been the focus. The problems of lead toxicity and organic solvents are not perfectly solved too. Spiro-OMeTAD is the most common HTL material, but it is expensive and unstable. Additives and structural engineering help it to promote stability. PEDOT:PSS and NiO are often used in inverted PSCs. Their efficiency is also unsatisfactory. Compared with the ETL, the research on the HTL is less. The reliability of the new HTL material needs to be improved. Non-precious metal electrode materials are becoming more and more popular to reduce costs. A variety of carbon materials and other materials are good choices. The stability of PSCs hinders commercialization, even now. The degradation mechanism needs to be deeply researched. Perhaps, simulation experiments can help with stability testing. Two-/three-dimensional PSCs have already shown attractive efficiencies. However, more efforts are needed to make them commercially viable. Of course, improving the performance of each functional layer one by one is not enough. The interaction between layers is also very important. The right materials and overall structure will pave the way for the development of PSCs. The world's first plant for the production of photovoltaic panels made of perovskites was opened in Poland in the town of Wroclaw two years ago. Perovskite photovoltaics from laboratory to industry is no longer a paper project [223].

Author Contributions: Conceptualization, Y.C. and M.Z.; validation, Y.C., M.Z., F.L. and Z.Y.; writing—original draft preparation, Y.C. and M.Z.; writing—review and editing, Y.C.; visualization, Y.C.; supervision, Y.C.; project administration, Y.C.; funding acquisition, Y.C. All authors have read and agreed to the published version of the manuscript.

Funding: This research was funded by the Natural Science Foundation of China, grant number 21701041, the Open Foundation of Hubei Collaborative Innovation Center for High-Efficiency Utilization of Solar Energy, grant number HBSKFQN2017001, and the Talents of the High-Level Scientific Research Foundation of the Hubei University of Technology, grant number BSQD2017010.

Institutional Review Board Statement: Not applicable.

Informed Consent Statement: Not applicable.

Data Availability Statement: No new data were created or analyzed in this study. Data sharing is available within the article.

Conflicts of Interest: The authors declare no conflict of interest.

References

1. Rabaia, M.K.H.; Abdelkareem, M.A.; Sayed, E.T.; Elsaid, K.; Chae, K.-J.; Wilberforce, T.; Olabi, A.G. Environmental impacts of solar energy systems: A review. *Sci. Total Environ.* **2021**, *754*, 141989. [CrossRef] [PubMed]
2. Zhao, X.; Liu, T.; Loo, Y.-L. Advancing 2D Perovskites for Efficient and Stable Solar Cells: Challenges and Opportunities. *Adv. Mater.* **2022**, *34*, 2105849. [CrossRef]
3. Xu, L.; Yuan, S.; Ma, L.; Zhang, B.; Fang, T.; Li, X.; Song, J. All-inorganic perovskite quantum dots as light-harvesting, interfacial, and light-converting layers toward solar cells. *J. Mater. Chem. A* **2021**, *9*, 18947–18973. [CrossRef]
4. Xiang, W.; Tress, W. Review on Recent Progress of All-Inorganic Metal Halide Perovskites and Solar Cells. *Adv. Mater.* **2019**, *31*, 1902851. [CrossRef]
5. Wu, T.; Qin, Z.; Wang, Y.; Wu, Y.; Chen, W.; Zhang, S.; Cai, M.; Dai, S.; Zhang, J.; Liu, J.; et al. The Main Progress of Perovskite Solar Cells in 2020-2021. *Nano-Micro Lett.* **2021**, *13*, 152. [CrossRef] [PubMed]
6. Wang, Z.; Zhang, Z.; Xie, L.; Wang, S.; Yang, C.; Fang, C.; Hao, F. Recent Advances and Perspectives of Photostability for Halide Perovskite Solar Cells. *Adv. Opt. Mater.* **2022**, *10*, 2101822. [CrossRef]
7. Roy, P.; Ghosh, A.; Barclay, F.; Khare, A.; Cuce, E. Perovskite Solar Cells: A Review of the Recent Advances. *Coatings* **2022**, *12*, 1089. [CrossRef]
8. Park, J.; Kim, J.; Yun, H.-S.; Paik, M.J.; Noh, E.; Mun, H.J.; Kim, M.G.; Shin, T.J.; Seok, S.I. Controlled growth of perovskite layers with volatile alkylammonium chlorides. *Nature* **2023**. [CrossRef]
9. Borriello, I.; Cantele, G.; Ninno, D. Ab initio investigation of hybrid organic-inorganic perovskites based on tin halides. *Phys. Rev. B* **2008**, *77*, 235214. [CrossRef]
10. Li, H.; Zhang, W. Perovskite Tandem Solar Cells: From Fundamentals to Commercial Deployment. *Chem. Rev.* **2020**, *120*, 9835–9950. [CrossRef]
11. Kieslich, G.; Sun, S.; Cheetham, A.K. Solid-state principles applied to organic–inorganic perovskites: New tricks for an old dog. *Chem. Sci.* **2014**, *5*, 4712–4715. [CrossRef]
12. Kim, H.-S.; Im, S.H.; Park, N.-G. Organolead Halide Perovskite: New Horizons in Solar Cell Research. *J. Phys. Chem. C* **2014**, *118*, 5615–5625. [CrossRef]
13. Pang, S.; Hu, H.; Zhang, J.; Lv, S.; Yu, Y.; Wei, F.; Qin, T.; Xu, H.; Liu, Z.; Cui, G. $NH_2CH{=}NH_2PbI_3$: An Alternative Organolead Iodide Perovskite Sensitizer for Mesoscopic Solar Cells. *Chem. Mater.* **2014**, *26*, 1485–1491. [CrossRef]
14. Wang, Y.Q.; Fu, W.F.; Yan, J.L.; Chen, J.H.; Yang, W.T.; Chen, H.Z. Low-bandgap mixed tin-lead iodide perovskite with large grains for high performance solar cells. *J. Mater. Chem. A* **2018**, *6*, 13090–13095. [CrossRef]
15. Li, Y.; Sun, W.; Yan, W.; Ye, S.; Rao, H.; Peng, H.; Zhao, Z.; Bian, Z.; Liu, Z.; Zhou, H.; et al. 50% Sn-Based Planar Perovskite Solar Cell with Power Conversion Efficiency up to 13.6%. *Adv. Energy Mater.* **2016**, *6*, 1601353. [CrossRef]
16. Sahli, F.; Werner, J.; Kamino, B.A.; Braeuninger, M.; Monnard, R.; Paviet-Salomon, B.; Barraud, L.; Ding, L.; Leon, J.J.D.; Sacchetto, D.; et al. Fully textured monolithic perovskite/silicon tandem solar cells with 25.2% power conversion efficiency. *Nat. Mater.* **2018**, *17*, 820–826. [CrossRef]
17. Jaysankar, M.; Filipic, M.; Zielinski, B.; Schmager, R.; Song, W.; Qiu, W.; Paetzold, U.W.; Aernouts, T.; Debucquoy, M.; Gehlhaar, R.; et al. Perovskite-silicon tandem solar modules with optimised light harvesting. *Energy Environ. Sci.* **2018**, *11*, 1489–1498. [CrossRef]
18. Heo, J.H.; Im, S.H. $CH_3NH_3PbBr_3$-$CH_3NH_3PbI_3$ Perovskite-Perovskite Tandem Solar Cells with Exceeding 2.2 V Open Circuit Voltage. *Adv. Mater.* **2016**, *28*, 5121–5125. [CrossRef] [PubMed]
19. Jost, M.; Kegelmann, L.; Korte, L.; Albrecht, S. Monolithic Perovskite Tandem Solar Cells: A Review of the Present Status and Advanced Characterization Methods Toward 30% Efficiency. *Adv. Energy Mater.* **2020**, *10*, 1904102. [CrossRef]
20. Zhang, Y.; Gu, M.; Li, N.; Xu, Y.; Ling, X.; Wang, Y.; Zhou, S.; Li, F.; Yang, F.; Ji, K.; et al. Realizing solution-processed monolithic PbS QDs/perovskite tandem solar cells with high UV stability. *J. Mater. Chem. A* **2018**, *6*, 24693–24701. [CrossRef]
21. Meng, L.; You, J.; Guo, T.-F.; Yang, Y. Recent Advances in the Inverted Planar Structure of Perovskite Solar Cells. *Acc. Chem. Res.* **2016**, *49*, 155–165. [CrossRef] [PubMed]
22. Jeon, N.J.; Noh, J.H.; Kim, Y.C.; Yang, W.S.; Ryu, S.; Seok, S.I. Solvent engineering for high-performance inorganic-organic hybrid perovskite solar cells. *Nat. Mater.* **2014**, *13*, 897–903. [CrossRef] [PubMed]

23. Jeon, N.J.; Na, H.; Jung, E.H.; Yang, T.-Y.; Lee, Y.G.; Kim, G.; Shin, H.-W.; Seok, S.I.; Lee, J.; Seo, J. A fluorene-terminated hole-transporting material for highly efficient and stable perovskite solar cells. *Nat. Energy* **2018**, *3*, 682–689. [CrossRef]
24. Wu, W.-Q.; Chen, D.; Caruso, R.A.; Cheng, Y.-B. Recent progress in hybrid perovskite solar cells based on n-type materials. *J. Mater. Chem. A* **2017**, *5*, 10092–10109. [CrossRef]
25. Kim, Y.S.; Jin, H.J.; Jung, H.R.; Kim, J.; Nguyen, B.P.; Kim, J.; Jo, W. Reduced extrinsic recombination process in anatase and rutile TiO_2 epitaxial thin films for efficient electron transport layers. *Sci. Rep.* **2021**, *11*, 6810. [CrossRef]
26. Maniarasu, S.; Karthikeyan, V.; Korukonda, T.B.; Pradhan, S.C.; Soman, S.; Ramasamy, E.; Veerappan, G. Ambient processed perovskite sensitized porous TiO_2 nanorods for highly efficient and stable perovskite solar cells. *J. Alloys Compod.* **2021**, *884*, 161061. [CrossRef]
27. Singh, M.; Chiang, C.-H.; Boopathi, K.M.; Hanmandlu, C.; Li, G.; Wu, C.-G.; Lin, H.-C.; Chu, C.-W. A novel ball milling technique for room temperature processing of TiO_2 nanoparticles employed as the electron transport layer in perovskite solar cells and modules. *J. Mater. Chem. A* **2018**, *6*, 7114–7122. [CrossRef]
28. Sun, J.; Pascoe, A.R.; Meyer, S.; Wu, Q.; Della Gaspera, E.; Raga, S.R.; Zhang, T.; Nattestad, A.; Bach, U.; Cheng, Y.-B.; et al. Ultrasonic spray deposition of TiO_2 electron transport layers for reproducible and high efficiency hybrid perovskite solar cells. *Sol. Energy* **2019**, *188*, 697–705. [CrossRef]
29. Lewis, A.; Troughton, J.R.; Smith, B.; McGettrick, J.; Dunlop, T.; De Rossi, F.; Pockett, A.; Spence, M.; Carnie, M.J.; Watson, T.M.; et al. In-depth analysis of defects in TiO_2 compact electron transport layers and impact on performance and hysteresis of planar perovskite devices at low light. *Sol. Energy Mater. Sol. Cells* **2020**, *209*, 110448. [CrossRef]
30. Chen, D.; Su, A.; Li, X.; Pang, S.; Zhu, W.; Xi, H.; Chang, J.; Zhang, J.; Zhang, C.; Hao, Y. Efficient planar perovskite solar cells with low-temperature atomic layer deposited TiO_2 electron transport layer and interfacial modifier. *Sol. Energy* **2019**, *188*, 239–246. [CrossRef]
31. Shahiduzzaman, M.; Sakuma, T.; Kaneko, T.; Tomita, K.; Isomura, M.; Taima, T.; Umezu, S.; Iwamori, S. Oblique Electrostatic Inkjet-Deposited TiO_2 Electron Transport Layers for Efficient Planar Perovskite Solar Cells. *Sci. Rep.* **2019**, *9*, 19494. [CrossRef] [PubMed]
32. Buffiere, M.; Ali, K.; Fares, E.; Samara, A.; Shetty, A.R.; Al Hassan, O.; Belaidi, A. Inkjet-Printed Compact TiO_2 Electron Transport Layer for Perovskite Solar Cells. *Energy Technol.* **2020**, *8*, 2000330. [CrossRef]
33. Huckaba, A.J.; Garcia-Benito, I.; Kanda, H.; Shibayama, N.; Oveisi, E.; Nazeeruddin, M.K. Inkjet-Printed TiO_2/Fullerene Composite Films for Planar Perovskite Solar Cells. *Helv. Chim. Acta* **2020**, *103*, e2000044. [CrossRef]
34. Liu, B.; Sun, G.; Sun, Q.; Lv, Y.; Huang, M.; Qi, B. Low-temperature fabrication of perovskite solar cells using modified TiO_2 electron transport layer. *Mater. Sci. Semicon. Proc.* **2022**, *138*, 106303. [CrossRef]
35. Noori, L.; Hoseinpour, V.; Shariatinia, Z. Optimization of TiO_2 paste concentration employed as electron transport layers in fully ambient air processed perovskite solar cells with a low-cost architecture. *Ceram. Int.* **2022**, *48*, 320–336. [CrossRef]
36. Supraja, S.; Dileep, K.R.; Chundi, N.; Ramasamy, E.; Shanmugasundaram, S.; Veerappan, G. Influence of bi-phasic TiO_2 as a low-temperature curable electron transport layer for efficient perovskite solar cells. *Sol. Energy* **2022**, *247*, 308–314. [CrossRef]
37. Ma, S.; Ahn, J.; Oh, Y.; Kwon, H.-C.; Lee, E.; Kim, K.; Yun, S.-C.; Moon, J. Facile Sol Gel-Derived Craterlike Dual-Functioning TiO_2 Electron Transport Layer for High-Efficiency Perovskite Solar Cells. *ACS Appl. Mater. Interfaces* **2018**, *10*, 14649–14658. [CrossRef]
38. Wang, K.; Zhao, W.; Li, H.; Li, D.; Liu, Z.; Wang, D.; Liu, S. Oxidation, reduction, and inert gases plasma-modified defects in TiO_2 as electron transport layer for planar perovskite solar cells. *J. CO_2 Util.* **2019**, *32*, 46–52. [CrossRef]
39. Ranjan, S.; Ranjan, R.; Tyagi, A.; Rana, K.S.; Soni, A.; Kodali, H.K.; Dalal, V.; Singh, A.; Garg, A.; Nalwa, K.S.; et al. Low-Temperature Microwave Processed TiO_2 as an Electron Transport Layer for Enhanced Performance and Atmospheric Stability in Planar Perovskite Solar Cells. *ACS Appl. Energy Mater.* **2022**, *5*, 2679–2696. [CrossRef]
40. Wang, L.; Miao, Q.; Sun, Z.; Zhang, H.; Liu, Z.; Wang, G.; Zhang, S. In Situ Electron Transport Layers by a Carboxyl Ionic Liquid-Assisted Microwave Technique for a 20.1% Perovskite Solar Cell. *ACS Appl. Energy Mater.* **2021**, *4*, 12112–12120. [CrossRef]
41. Jarwal, D.K.; Kumar, A.; Mishra, A.K.; Ratan, S.; Kumar, C.; Upadhyay, D.; Mukherjee, B.; Jit, S. Efficiency Improvement of TiO_2 Nanorods Electron Transport Layer Based Perovskite Solar Cells by Solvothermal Etching. *IEEE J. Photovolt.* **2019**, *9*, 1699–1707. [CrossRef]
42. Shahvaranfard, F.; Altomare, M.; Hou, Y.; Hejazi, S.; Meng, W.; Osuagwu, B.; Li, N.; Brabec, C.J.; Schmuki, P. Engineering of the Electron Transport Layer/Perovskite Interface in Solar Cells Designed on TiO_2 Rutile Nanorods. *Adv. Funct. Mater.* **2020**, *30*, 1909738. [CrossRef]
43. Lu, H.; Zhong, J.; Ji, C.; Zhao, J.; Li, D.; Zhao, R.; Jiang, Y.; Fang, S.; Liang, T.; Li, H.; et al. Fabricating an optimal rutile TiO_2 electron transport layer by delicately tuning $TiCl_4$ precursor solution for high performance perovskite solar cells. *Nano Energy* **2020**, *68*, 104336. [CrossRef]
44. Amalathas, A.P.; Landova, L.; Conrad, B.; Holovsky, J. Concentration-Dependent Impact of Alkali Li Metal Doped Mesoporous TiO_2 Electron Transport Layer on the Performance of $CH_3NH_3PbI_3$ Perovskite Solar Cells. *J. Phys. Chem. C* **2019**, *123*, 19376–19384. [CrossRef]
45. Arshad, Z.; Khoja, A.H.; Shakir, S.; Afzal, A.; Mujtaba, M.A.; Soudagar, M.E.M.; Fayaz, H.; Saleel, C.A.; Farukh, S.; Saeed, M. Magnesium doped TiO_2 as an efficient electron transport layer in perovskite solar cells. *Case Stud. Therm. Eng.* **2021**, *26*, 101101. [CrossRef]

46. Liu, X.; Wu, Z.; Zhang, Y.; Tsamis, C. Low temperature Zn-doped TiO_2 as electron transport layer for 19% efficient planar perovskite solar cells. *Appl. Surf. Sci.* **2019**, *471*, 28–35. [CrossRef]
47. Lv, Y.; Tong, H.; Cai, W.; Zhang, Z.; Chen, H.; Zhou, X. Boosting the efficiency of commercial available carbon-based perovskite solar cells using Zinc-doped TiO_2 nanorod arrays as electron transport layer. *J. Alloys Compod.* **2021**, *851*, 156785. [CrossRef]
48. Ren, W.; Liu, Y.; Wu, Y.; Sun, Q.; Cui, Y.; Hao, Y. Interface modification of an electron transport layer using europium acetate for enhancing the performance of P_3HT-based inorganic perovskite solar cells. *Phys. Chem. Chem. Phys.* **2021**, *23*, 23818–23826. [CrossRef]
49. Sanehira, Y.; Shibayama, N.; Numata, Y.; Ikegami, M.; Miyasaka, T. Low-Temperature Synthesized Nb-Doped TiO_2 Electron Transport Layer Enabling High-Efficiency Perovskite Solar Cells by Band Alignment Tuning. *ACS Appl. Mater. Interfaces* **2020**, *12*, 15175–15182. [CrossRef]
50. Jin, J.; Li, H.; Bi, W.; Chen, C.; Zhang, B.; Xu, L.; Dong, B.; Song, H.; Dai, Q. Efficient and stable perovskite solar cells through e-beam preparation of cerium doped TiO_2 electron transport layer, ultraviolet conversion layer $CsPbBr_3$ and the encapsulation layer Al_2O_3. *Sol. Energy* **2020**, *198*, 187–193. [CrossRef]
51. Xu, R.; Li, Y.; Feng, S.; Wang, J.; Zhang, J.; Zhang, X.; Bian, C.; Fu, W.; Li, Z.; Yang, H. Enhanced performance of planar perovskite solar cells using Ce-doped TiO_2 as electron transport layer. *J. Mater. Sci.* **2020**, *55*, 5681–5689. [CrossRef]
52. Qureshi, A.A.; Javed, H.M.A.; Javed, S.; Bashir, A.; Usman, M.; Akram, A.; Ahmad, M.I.; Ali, U.; Shahid, M.; Rizwan, M.; et al. Incorporation of Zr-doped TiO_2 nanoparticles in electron transport layer for efficient planar perovskite solar cells. *Surf. Interfaces* **2021**, *25*, 101299. [CrossRef]
53. Sandhu, S.; Saharan, C.; Buruga, S.K.; Kumar, S.A.; Rana, P.S.; Nagajyothi, P.C.; Mane, S.D. Micro structurally engineered hysteresis-free high efficiency perovskite solar cell using Zr-doped TiO_2 electron transport layer. *Ceram. Int.* **2021**, *47*, 14665–14672. [CrossRef]
54. Chen, K.-T.; Hsu, C.-H.; Jiang, S.-C.; Liang, L.-S.; Gao, P.; Qiu, Y.; Wu, W.-Y.; Zhang, S.; Zhu, W.-Z.; Lien, S.-Y. Effect of Annealing Temperature on Tantalum-Doped TiO_2 as Electron Transport Layer in Perovskite Solar Cells. *IEEE Trans. Electron Devices* **2022**, *69*, 1149–1154. [CrossRef]
55. Culu, A.; Kaya, I.C.; Sonmezoglu, S. Spray-Pyrolyzed Tantalium-Doped TiO_2 Compact Electron Transport Layer for UV-Photostable Planar Perovskite Solar Cells Exceeding 20% Efficiency. *ACS Appl. Energy Mater.* **2022**, *5*, 3454–3462. [CrossRef]
56. Ebrahimi, M.; Kermanpur, A.; Atapour, M.; Adhami, S.; Heidari, R.H.; Khorshidi, E.; Irannejad, N.; Rezaie, B. Performance enhancement of mesoscopic perovskite solar cells with GQDs-doped TiO_2 electron transport layer. *Sol. Energy Mater. Sol. Cells* **2020**, *208*, 110407. [CrossRef]
57. Liu, Z.; Sun, B.; Liu, X.; Han, J.; Ye, H.; Tu, Y.; Chen, C.; Shi, T.; Tang, Z.; Liao, G. 15% efficient carbon based planar-heterojunction perovskite solar cells using a TiO_2/SnO_2 bilayer as the electron transport layer. *J. Mater. Chem. A* **2018**, *6*, 7409–7419. [CrossRef]
58. Mali, S.S.; Patil, J.V.; Arandiyan, H.; Hong, C.K. Reduced methylammonium triple-cation $Rb_{0.05}(FAPbI_3)_{0.95}(MAPbBr_3)_{0.05}$ perovskite solar cells based on a TiO_2/SnO_2 bilayer electron transport layer approaching a stabilized 21% efficiency: The role of antisolvents. *J. Mater. Chem. A* **2019**, *7*, 17516–17528. [CrossRef]
59. Xie, H.; Yin, X.; Liu, J.; Guo, Y.; Chen, P.; Que, W.; Wang, G.; Gao, B. Low temperature solution-derived TiO_2-SnO_2 bilayered electron transport layer for high performance perovskite solar cells. *Appl. Surf. Sci.* **2019**, *464*, 700–707. [CrossRef]
60. Mohammadbeigi, A.; Mozaffari, S.; Ghorashi, S.M.B. Yolk-shell SnO_2@TiO_2 nanospheres as electron transport layer in mesoscopic perovskite solar cell. *J. Sol-Gel Sci. Technol.* **2020**, *94*, 731–742. [CrossRef]
61. Li, N.; Yan, J.; Ai, Y.; Jiang, E.; Lin, L.; Shou, C.; Yan, B.; Sheng, J.; Ye, J. A low-temperature TiO_2/SnO_2 electron transport layer for high-performance planar perovskite solar cells. *Sci. China Mater.* **2020**, *63*, 207–215. [CrossRef]
62. Chiang, C.H.; Kan, C.W.; Wu, C.G. Synergistic Engineering of Conduction Band, Conductivity, and Interface of Bilayered Electron Transport Layers with Scalable TiO_2 and SnO_2 Nanoparticles for High-Efficiency Stable Perovskite Solar Cells. *ACS Appl. Mater. Interfaces* **2021**, *13*, 23606–23615. [CrossRef] [PubMed]
63. Koech, R.K.; Ichwani, R.; Oyewole, D.; Kigozi, M.; Amune, D.; Sanni, D.M.; Adeniji, S.; Oyewole, K.; Bello, A.; Ntsoenzok, E.; et al. Tin Oxide Modified Titanium Dioxide as Electron Transport Layer in Formamidinium-Rich Perovskite Solar Cells. *Energies* **2021**, *14*, 7870. [CrossRef]
64. Ko, Y.; Kim, T.; Lee, C.; Lee, C.; Yun, Y.J.; Jun, Y. Alleviating Interfacial Recombination of Heterojunction Electron Transport Layer via Oxygen Vacancy Engineering for Efficient Perovskite Solar Cells Over 23%. *Energy Environ. Mater.* **2022**, *0*, 1–12. [CrossRef]
65. Paik, M.J.; Yoo, J.W.; Park, J.; Noh, E.; Kim, H.; Ji, S.-G.; Kim, Y.Y.; Il Seok, S. SnO_2-TiO_2 Hybrid Electron Transport Layer for Efficient and Flexible Perovskite Solar Cells. *ACS Energy Lett.* **2022**, *7*, 1864–1870. [CrossRef]
66. Zhou, J.; Lyu, M.; Zhu, J.; Li, G.; Li, Y.; Jin, S.; Song, J.; Niu, H.; Xu, J.; Zhou, R. SnO_2 Quantum Dot-Modified Mesoporous TiO_2 Electron Transport Layer for Efficient and Stable Perovskite Solar Cells. *ACS Appl. Energy Mater.* **2022**, *5*, 3052–3063. [CrossRef]
67. Wang, D.; Ni, J.; Guan, J.; Zhou, X.; Zhang, S.; Zhang, Y.; Huang, Q.; Cai, H.; Li, J.; Zhang, J. Thin Film of TiO_2-ZnO Binary Mixed Nanoparticles as Electron Transport Layers in Low-Temperature Processed Perovskite Solar Cells. *Nano* **2020**, *15*, 2050036. [CrossRef]
68. Yue, M.; Su, J.; Zhao, P.; Lin, Z.H.; Zhang, J.C.; Chang, J.J.; Hao, Y. Optimizing the Performance of $CsPbI_3$-Based Perovskite Solar Cells via Doping a ZnO Electron Transport Layer Coupled with Interface Engineering. *Nano-Micro Lett.* **2019**, *11*, 91. [CrossRef]

69. Wang, F.Y.; Yang, M.F.; Zhang, Y.H.; Du, J.Y.; Han, D.L.; Yang, L.L.; Fan, L.; Sui, Y.R.; Sun, Y.F.; Meng, X.W.; et al. Constructing m-TiO_2/a-WOx hybrid electron transport layer to boost interfacial charge transfer for efficient perovskite solar cells. *Chem. Eng. J.* **2020**, *402*, 126303. [CrossRef]
70. You, Y.; Tian, W.; Min, L.; Cao, F.; Deng, K.; Li, L. TiO_2/WO_3 Bilayer as Electron Transport Layer for Efficient Planar Perovskite Solar Cell with Efficiency Exceeding 20%. *Adv. Mater. Interfaces* **2020**, *7*, 1901406. [CrossRef]
71. Dadashbeik, M.; Fathi, D.; Eskandari, M. Design and simulation of perovskite solar cells based on graphene and TiO_2/graphene nanocomposite as electron transport layer. *Sol. Energy* **2020**, *207*, 917–924. [CrossRef]
72. Mohseni, H.R.; Dehghanipour, M.; Dehghan, N.; Tamaddon, F.; Ahmadi, M.; Sabet, M.; Behjat, A. Enhancement of the photovoltaic performance and the stability of perovskite solar cells via the modification of electron transport layers with reduced graphene oxide/polyaniline composite. *Sol. Energy* **2021**, *213*, 59–66. [CrossRef]
73. Zhao, Y.; Zhang, H.; Ren, X.G.; Zhu, H.L.; Huang, Z.F.; Ye, F.; Ouyang, D.; Cheah, K.W.; Jen, A.K.Y.; Choy, W.C.H. Thick TiO_2-Based Top Electron Transport Layer on Perovskite for Highly Efficient and Stable Solar Cells. *ACS Energy Lett.* **2018**, *3*, 2891–2898. [CrossRef]
74. Zhang, X.; Zhang, W.; Wu, T.; Wu, J.; Lan, Z. High efficiency and negligible hysteresis planar perovskite solar cells based on NiO nanocrystals modified TiO_2 electron transport layers. *Sol. Energy* **2019**, *181*, 293–300. [CrossRef]
75. Cao, T.; Chen, K.; Chen, Q.; Zhou, Y.; Chen, N.; Li, Y. Fullerene Derivative-Modified SnO_2 Electron Transport Layer for Highly Efficient Perovskite Solar Cells with Efficiency over 21%. *ACS Appl. Mater. Interfaces* **2019**, *11*, 33825–33834. [CrossRef]
76. Liang, J.; Chen, Z.; Yang, G.; Wang, H.; Ye, F.; Tao, C.; Fang, G. Achieving High Open-Circuit Voltage on Planar Perovskite Solar Cells via Chlorine-Doped Tin Oxide Electron Transport Layers. *ACS Appl. Mater. Interfaces* **2019**, *11*, 23152–23159. [CrossRef]
77. Jiang, E.; Ai, Y.; Yan, J.; Li, N.; Lin, L.; Wang, Z.; Shou, C.; Yan, B.; Zeng, Y.; Sheng, J.; et al. Phosphate-Passivated SnO_2 Electron Transport Layer for High-Performance Perovskite Solar Cells. *ACS Appl. Mater. Interfaces* **2019**, *11*, 36727–36734. [CrossRef]
78. Wang, J.; Datta, K.; Weijtens, C.H.L.; Wienk, M.M.; Janssen, R.A.J. Insights into Fullerene Passivation of SnO_2 Electron Transport Layers in Perovskite Solar Cells. *Adv. Funct. Mater.* **2019**, *29*, 1905883. [CrossRef]
79. Cao, W.; Zhang, J.; Lin, K.; Qiu, L.; Li, J.; Dong, Y.; Wang, J.; Xia, D.; Fan, R.; Yang, Y. Enhanced Charge Transport and Interface Passivation in Efficient Perovskite Solar Cells Using Sulfur-Doped Graphite Carbon Nitride-Modified SnO_2-Based Electron Transport Layers. *Sol. RRL* **2021**, *5*, 2100058. [CrossRef]
80. Liu, C.; Su, H.; Xie, K.; Wang, H.; Zhai, P.; Chang, N.; Zhang, S.; Ban, Q.; Guo, M.; Zhang, J.; et al. Highly Enhanced Efficiency of Planar Perovskite Solar Cells by an Electron Transport Layer Using Phytic Acid-Complexed SnO_2 Colloids. *Sol. RRL* **2021**, *5*, 2100067. [CrossRef]
81. Lin, Z.C.; Zhang, W.Q.; Cai, Q.B.; Xu, X.N.; Dong, H.Y.; Mu, C.; Zhang, J.P. Precursor Engineering of the Electron Transport Layer for Application in High-Performance Perovskite Solar Cells. *Adv. Sci.* **2021**, *8*, 2102845. [CrossRef] [PubMed]
82. Li, X.; Shi, Z.; Behrouznejad, F.; Hatamvand, M.; Zhang, X.; Wang, Y.; Liu, F.; Wang, H.; Liu, K.; Dong, H.; et al. Highly efficient flexible perovskite solar cells with vacuum-assisted low-temperature annealed SnO_2 electron transport layer. *J. Energy Chem.* **2022**, *67*, 1–7. [CrossRef]
83. Liu, C.; Guo, M.; Su, H.; Zhai, P.; Xie, K.; Liu, Z.; Zhang, J.; Liu, L.; Fu, H. Highly improved efficiency and stability of planar perovskite solar cells via bifunctional phytic acid dipotassium anchored SnO_2 electron transport layer. *Appl. Surf. Sci.* **2022**, *588*, 152943. [CrossRef]
84. Xu, Z.; Zhou, X.; Li, X.; Zhang, P. Polymer-Regulated SnO_2 Composites Electron Transport Layer for High-Efficiency n-i-p Perovskite Solar Cells. *Sol. RRL* **2022**, *6*, 2200092. [CrossRef]
85. Xu, Z.; Ng, C.H.; Zhou, X.; Li, X.; Zhang, P.; Teo, S.H. Polymer-complexed SnO_2 electron transport layer for high-efficiency n-i-p perovskite solar cells. *Nanoscale* **2022**, *14*, 12090–12098. [CrossRef]
86. Zong, B.; Deng, J.; Sun, Q.; Zhang, Z.; Meng, X.; Shen, B.; Kang, B.; Silva, S.R.P.; Lu, G. Facile Surface Engineering of Composite Electron Transport Layer for Highly Efficient Perovskite Solar Cells with a Fill Factor Exceeding 81%. *Adv. Mater. Interfaces* **2022**, *9*, 2102331. [CrossRef]
87. Zong, B.; Sun, Q.; Deng, J.; Meng, X.; Zhang, Z.; Kang, B.; Silva, S.R.P.; Lu, G. Multi-cation hybrid stannic oxide electron transport layer for high-efficiency perovskite solar cells. *J. Colloid Interface Sci.* **2022**, *614*, 415–424. [CrossRef]
88. Gu, L.; Wang, C.; Mo, W.; Zeng, H.; Shou, C.; Yang, S.; Wen, F. High efficiency perovskite solar cells via NaCl modified tin oxide electron transport layer. *Org. Electron.* **2023**, *113*, 106677. [CrossRef]
89. Guo, Y.; Yin, X.; Liu, J.; Chen, W.; Wen, S.; Que, M.; Xie, H.; Yang, Y.; Que, W.; Gao, B. Vacuum thermal-evaporated SnO_2 as uniform electron transport layer and novel management of perovskite intermediates for efficient and stable planar perovskite solar cells. *Org. Electron.* **2019**, *65*, 207–214. [CrossRef]
90. Bai, G.; Wu, Z.; Li, J.; Bu, T.; Li, W.; Li, W.; Huang, F.; Zhang, Q.; Cheng, Y.-B.; Zhong, J. High performance perovskite sub-module with sputtered SnO_2 electron transport layer. *Sol. Energy* **2019**, *183*, 306–314. [CrossRef]
91. Kam, M.; Zhu, Y.; Zhang, D.; Gu, L.; Chen, J.; Fan, Z. Efficient Mixed-Cation Mixed-Halide Perovskite Solar Cells by All-Vacuum Sequential Deposition Using Metal Oxide Electron Transport Layer. *Sol. RRL* **2019**, *3*, 1900050. [CrossRef]
92. Kam, M.; Zhang, Q.P.; Zhang, D.Q.; Fan, Z.Y. Room-Temperature Sputtered SnO_2 as Robust Electron Transport Layer for Air-Stable and Efficient Perovskite Solar Cells on Rigid and Flexible Substrates. *Sci. Rep.* **2019**, *9*, 6963. [CrossRef] [PubMed]

93. Qiu, L.; Liu, Z.; Ono, L.K.; Jiang, Y.; Son, D.-Y.; Hawash, Z.; He, S.; Qi, Y. Scalable Fabrication of Stable High Efficiency Perovskite Solar Cells and Modules Utilizing Room Temperature Sputtered SnO_2 Electron Transport Layer. *Adv. Funct. Mater.* **2019**, *29*, 1806779. [CrossRef]
94. Guan, J.; Ni, J.; Zhou, X.; Liu, Y.; Yin, J.; Wang, J.; Wang, D.; Zhang, Y.; Li, J.; Cai, H.; et al. High-Performance Electron Transport Layer via Ultrasonic Spray Deposition for Commercialized Perovskite Solar Cells. *ACS Appl. Energy Mater.* **2020**, *3*, 11570–11580. [CrossRef]
95. Kumar, N.; Lee, H.B.; Sahani, R.; Tyagi, B.; Cho, S.; Lee, J.-S.; Kang, J.-W. Room-Temperature Spray Deposition of Large-Area SnO_2 Electron Transport Layer for High Performance, Stable FAPbI(3)-Based Perovskite Solar Cells. *Small Methods* **2022**, *6*, 2101127. [CrossRef] [PubMed]
96. Erdenebileg, E.; Wang, H.; Li, J.; Singh, N.; Dewi, H.A.; Tiwari, N.; Mathews, N.; Mhaisalkar, S.; Bruno, A. Low-Temperature Atomic Layer Deposited Electron Transport Layers for Co-Evaporated Perovskite Solar Cells. *Sol. RRL* **2022**, *6*, 2100842. [CrossRef]
97. Liu, C.; Zhang, L.; Zhou, X.; Gao, J.; Chen, W.; Wang, X.; Xu, B. Hydrothermally Treated SnO_2 as the Electron Transport Layer in High-Efficiency Flexible Perovskite Solar Cells with a Certificated Efficiency of 17.3%. *Adv. Funct. Mater.* **2019**, *29*, 1807604. [CrossRef]
98. Liu, J.; Li, S.; Liu, S.; Chu, Y.; Ye, T.; Qiu, C.; Qiu, Z.; Wang, X.; Wang, Y.; Su, Y.; et al. Oxygen Vacancy Management for High-Temperature Mesoporous SnO_2 Electron Transport Layers in Printable Perovskite Solar Cells. *Angew. Chem. Int. Ed.* **2022**, *61*, e202202012. [CrossRef]
99. Ma, Z.; Zhou, W.; Xiao, Z.; Zhang, H.; Li, Z.; Zhuang, J.; Pen, C.; Huang, Y. Negligible hysteresis planar perovskite solar cells using Ga-doped SnO_2 nanocrystal as electron transport layers. *Org. Electron.* **2019**, *71*, 98–105. [CrossRef]
100. Zhao, Y.; Deng, Q.; Guo, R.; Wu, Z.; Li, Y.; Duan, Y.; Shen, Y.; Zhang, W.; Shao, G. Sputtered Ga-Doped SnO_x Electron Transport Layer for Large-Area All-Inorganic Perovskite Solar Cells. *ACS Appl. Mater. Interfaces* **2020**, *12*, 54904–54915. [CrossRef] [PubMed]
101. Liu, Q.; Zhang, X.; Li, C.; Lu, H.; Weng, Z.; Pan, Y.; Chen, W.; Hang, X.-C.; Sun, Z.; Zhan, Y. Effect of tantalum doping on SnO_2 electron transport layer via low temperature process for perovskite solar cells. *Appl. Phys. Lett.* **2019**, *115*, 143903. [CrossRef]
102. Song, J.; Xu, X.; Wu, J.; Lan, Z. Low-temperature solution-processing high quality Nb-doped SnO_2 nanocrystals-based electron transport layers for efficient planar perovskite solar cells. *Funct. Mater. Lett.* **2019**, *12*, 1850091. [CrossRef]
103. Guo, R.X.; Zhao, Y.; Zhang, Y.S.; Deng, Q.R.; Shen, Y.L.; Zhang, W.; Shao, G.S. Significant performance enhancement of all-inorganic CsPbBr3 perovskite solar cells enabled by Nb-doped SnO_2 as effective electron transport layer. *Energy Environ. Mater.* **2021**, *4*, 671–680. [CrossRef]
104. Ye, H.; Liu, Z.; Liu, X.; Sun, B.; Tan, X.; Tu, Y.; Shi, T.; Tang, Z.; Liao, G. 17.78% efficient low-temperature carbon-based planar perovskite solar cells using Zn-doped SnO_2 electron transport layer. *Appl. Surf. Sci.* **2019**, *478*, 417–425. [CrossRef]
105. Qiang, Y.; Xie, Y.; Qi, Y.; Wei, P.; Shi, H.; Geng, C.; Liu, H. Enhanced performance of carbon-based perovskite solar cells with a Li^+-doped SnO_2 electron transport layer and Al_2O_3 scaffold layer. *Sol. Energy* **2020**, *201*, 523–529. [CrossRef]
106. Tian, J.; Zhang, J.; Li, X.; Cheng, B.; Yu, J.; Ho, W. Low-Temperature-Processed Zr/F Co-Doped SnO_2 Electron Transport Layer for High-Efficiency Planar Perovskite Solar Cells. *Sol. RRL* **2020**, *4*, 2000090. [CrossRef]
107. Zhang, S.; Gu, H.; Chen, S.-C.; Zheng, Q. KF-Doped SnO_2 as an electron transport layer for efficient inorganic $CsPbI_2Br$ perovskite solar cells with enhanced open-circuit voltages. *J. Mater. Chem. C* **2021**, *9*, 4240–4247. [CrossRef]
108. Wu, J.-B.; Zhen, C.; Liu, G. Photo-assisted Cl doping of SnO_2 electron transport layer for hysteresis-less perovskite solar cells with enhanced efficiency. *Rare Met.* **2022**, *41*, 361–367. [CrossRef]
109. Ye, J.; Li, Y.; Medjahed, A.A.; Pouget, S.; Aldakov, D.; Liu, Y.; Reiss, P. Doped Bilayer Tin(IV) Oxide Electron Transport Layer for High Open-Circuit Voltage Planar Perovskite Solar Cells with Reduced Hysteresis. *Small* **2021**, *17*, 2005671. [CrossRef] [PubMed]
110. Pang, S.; Zhang, C.; Zhang, H.; Dong, H.; Chen, D.; Zhu, W.; Xi, H.; Chang, J.; Lin, Z.; Zhang, J.; et al. Boosting performance of perovskite solar cells with Graphene quantum dots decorated SnO_2 electron transport layers. *Appl. Surf. Sci.* **2020**, *507*, 145099. [CrossRef]
111. Mohamadkhani, F.; Javadpour, S.; Taghavinia, N. Improvement of planar perovskite solar cells by using solution processed SnO_2/CdS as electron transport layer. *Sol. Energy* **2019**, *191*, 647–653. [CrossRef]
112. Yang, L.; Dall'Agnese, Y.; Hantanasirisakul, K.; Shuck, C.E.; Maleski, K.; Alhabeb, M.; Chen, G.; Gao, Y.; Sanehira, Y.; Jena, A.K.; et al. SnO_2-Ti_3C_2 MXene electron transport layers for perovskite solar cells. *J. Mater. Chem. A* **2019**, *7*, 5635–5642. [CrossRef]
113. Noh, Y.W.; Jin, I.S.; Kim, K.S.; Park, S.H.; Jung, J.W. Reduced energy loss in SnO_2/ZnO bilayer electron transport layer-based perovskite solar cells for achieving high efficiencies in outdoor/indoor environments. *J. Mater. Chem. A* **2020**, *8*, 17163–17173. [CrossRef]
114. Khan, U.; Iqbal, T.; Khan, M.; Wu, R. SnO_2/ZnO as double electron transport layer for halide perovskite solar cells. *Sol. Energy* **2021**, *223*, 346–350. [CrossRef]
115. He, R.Q.; Nie, S.Q.; Huang, X.F.; Wu, Y.Z.; Chen, R.H.; Yin, J.; Wu, B.H.; Li, J.; Zheng, N.F. Scalable Preparation of High-Performance ZnO-SnO_2 Cascaded Electron Transport Layer for Efficient Perovskite Solar Modules. *Sol. RRL* **2022**, *6*, 2100639. [CrossRef]
116. Luo, X.; Gao, Y.; Zhu, P.; Han, Q.; Lin, R.; Gao, H.; Wang, Y.; Zhu, J.; Li, S.; Tan, H. Record Photocurrent Density over 26 mA $cm^{(-2)}$ in Planar Perovskite Solar Cells Enabled by Antireflective Cascaded Electron Transport Layer. *Sol. RRL* **2020**, *4*, 2000169. [CrossRef]

117. Liu, B.-T.; Zhang, Y.-Z.; Zuo, Y.-Y.; Rachmawati, D. Passivation and energy-level change of the SnO_2 electron transport layer by reactive titania for perovskite solar cells. *J. Alloys Compod.* **2022**, *929*, 167349. [CrossRef]
118. Tang, H.; Cao, Q.; He, Z.; Wang, S.; Han, J.; Li, T.; Gao, B.; Yang, J.; Deng, D.; Li, X. SnO_2-Carbon Nanotubes Hybrid Electron Transport Layer for Efficient and Hysteresis-Free Planar Perovskite Solar Cells. *Sol. RRL* **2020**, *4*, 1900415. [CrossRef]
119. Zhu, P.; Gu, S.; Luo, X.; Gao, Y.; Li, S.; Zhu, J.; Tan, H. Simultaneous Contact and Grain-Boundary Passivation in Planar Perovskite Solar Cells Using SnO_2-KCl Composite Electron Transport Layer. *Adv. Energy Mater.* **2020**, *10*, 1903083. [CrossRef]
120. Zhou, J.; Zhou, R.; Zhu, J.; Jiang, P.; Wan, L.; Niu, H.; Hu, L.; Yang, X.; Xu, J.; Xu, B. Colloidal SnO_2-Assisted CdS Electron Transport Layer Enables Efficient Electron Extraction for Planar Perovskite Solar Cells. *Sol. RRL* **2021**, *5*, 2100494. [CrossRef]
121. Zhao, R.; Wang, L.; Huang, J.; Miao, X.; Sun, L.; Hua, Y.; Wang, Y. Amino-capped zinc oxide modified tin oxide electron transport layer for efficient perovskite solar cells. *Cell Rep. Phys. Sci.* **2021**, *2*, 100590. [CrossRef]
122. Zhang, J.; Tan, C.H.; Du, T.; Morbidoni, M.; Lin, C.-T.; Xu, S.; Durrant, J.R.; McLachlan, M.A. ZnO-PCBM bilayers as electron transport layers in low-temperature processed perovskite solar cells. *Sci. Bull.* **2018**, *63*, 343–348. [CrossRef]
123. Zhang, J.; Morbidoni, M.; Huang, K.; Feng, S.; McLachlan, M.A. Environmentally friendly, aqueous processed ZnO as an efficient electron transport layer for low temperature processed metal-halide perovskite photovoltaics. *Inorg. Chem. Front.* **2018**, *5*, 84–89. [CrossRef]
124. Zhao, W.; Li, H.; Li, D.; Liu, Z.; Wang, D.; Liu, S. Comprehensive investigation of sputtered and spin-coated zinc oxide electron transport layers for highly efficient and stable planar perovskite solar cells. *J. Power Sources* **2019**, *427*, 223–230. [CrossRef]
125. Yang, Z.; Fan, Q.; Shen, T.; Jin, J.; Deng, W.; Xin, J.; Huang, X.; Wang, X.; Li, J. Amine-passivated ZnO electron transport layer for thermal stability-enhanced perovskite solar cells. *Sol. Energy* **2020**, *204*, 223–230. [CrossRef]
126. Eswaramoorthy, N.; Rajaram, K. Planar perovskite solar cells: Plasmonic nanoparticles-modified ZnO as an electron transport layer for enhancing the device performance and stability at ambient conditions. *Int. J. Energy Res.* **2022**, *46*, 10724–10740. [CrossRef]
127. Adnan, M.; Usman, M.; Ali, S.; Javed, S.; Islam, M.; Akram, M.A. Aluminum Doping Effects on Interface Depletion Width of Low Temperature Processed ZnO Electron Transport Layer-Based Perovskite Solar Cells. *Front. Chem.* **2022**, *9*, 795291. [CrossRef]
128. Bouhjar, F.; Derbali, L.; Mari, B. High performance novel flexible perovskite solar cell based on a low-cost-processed ZnO:Co electron transport layer. *Nano Res.* **2020**, *13*, 2546–2555. [CrossRef]
129. Ierides, I.; Ligorio, G.; McLachlan, M.A.; Guo, K.; List-Kratochvil, E.J.W.; Cacialli, F. Inverted organic photovoltaics with a solution-processed Mg-doped ZnO electron transport layer annealed at 150 degrees C. *Sustain. Energy Fuels* **2022**, *6*, 2835–2845. [CrossRef]
130. Arshad, Z.; Wageh, S.; Maiyalagan, T.; Ali, M.; Arshad, U.; Noor ul, a.; Qadir, M.B.; Mateen, F.; Al-Sehemi, A.G. Enhanced charge transport characteristics in zinc oxide nanofibers via Mg^{2+} doping for electron transport layer in perovskite solar cells and antibacterial textiles. *Ceram. Int.* **2022**, *48*, 24363–24371. [CrossRef]
131. Bagha, G.; Mersagh, M.R.; Naffakh-Moosavy, H.; Matin, L.F. The role of rGO sheet and Ag dopant in reducing ZnO electron transport layer recombination in planar perovskite solar cells. *Ceram. Int.* **2021**, *47*, 16111–16123. [CrossRef]
132. Pang, Z.; Yang, S.; Sun, Y.; He, L.; Wang, F.; Fan, L.; Chi, S.; Sun, X.; Yang, L.; Yang, J. Hydrophobic PbS QDs layer decorated ZnO electron transport layer to boost photovoltaic performance of perovskite solar cells. *Chem. Eng. J.* **2022**, *439*, 135701. [CrossRef]
133. Valsalakumar, S.; Roy, A.; Mallick, T.K.; Hinshelwood, J.; Sundaram, S. An Overview of Current Printing Technologies for Large-Scale Perovskite Solar Cell Development. *Energies* **2023**, *16*, 190. [CrossRef]
134. Im, J.-H.; Kim, H.-S.; Park, N.-G. Morphology-photovoltaic property correlation in perovskite solar cells: One-step versus two-step deposition of $CH_3NH_3PbI_3$. *APL Mater.* **2014**, *2*, 081510. [CrossRef]
135. Cheng, J.; Liu, F.; Tang, Z.Q.; Li, Y.L. Scalable Blade Coating: A Technique Accelerating the Commercialization of Perovskite-Based Photovoltaics. *Energy Technol.* **2021**, *9*, 2100204. [CrossRef]
136. Jiang, Y.; He, S.; Qiu, L.; Zhao, Y.; Qi, Y. Perovskite solar cells by vapor deposition based and assisted methods. *Appl. Phys. Rev.* **2022**, *9*, 21305. [CrossRef]
137. Roy, P.; Sinha, N.K.; Tiwari, S.; Khare, A. A review on perovskite solar cells: Evolution of architecture, fabrication techniques, commercialization issues and status. *Sol. Energy* **2020**, *198*, 665–688. [CrossRef]
138. Huang, F.; Li, M.; Siffalovic, P.; Cao, G.; Tian, J. From scalable solution fabrication of perovskite films towards commercialization of solar cells. *Energy Environ. Sci.* **2019**, *12*, 518–549. [CrossRef]
139. Zuo, C.T.; Scully, A.D.; Gao, M. Drop-Casting Method to Screen Ruddlesden-Popper Perovskite Formulations for Use in Solar Cells. *ACS Appl. Mater. Interfaces* **2021**, *13*, 56217–56225. [CrossRef]
140. Zuo, C.A.T.; Ding, L.M. Drop-Casting to Make Efficient Perovskite Solar Cells under High Humidity. *Angew. Chem.* **2021**, *60*, 11242–11246. [CrossRef]
141. Kumar, A.; Shkir, M.; Somaily, H.H.; Singh, K.L.; Choudhary, B.C.; Tripathi, S.K. A simple, low-cost modified drop-casting method to develop high-quality $CH_3NH_3PbI_3$ perovskite thin films. *Phys. B* **2022**, *630*, 413678. [CrossRef]
142. Irshad, Z.; Adnan, M.; Lee, J.K. Simple preparation of highly efficient $MA_xFA_{1-x}PbI_3$ perovskite films from an aqueous halide-free lead precursor by all dip-coating approach and application in high-performance perovskite solar cells. *J. Mater. Sci.* **2022**, *57*, 1936–1946. [CrossRef]
143. Adnan, M.; Lee, J.K. Highly efficient planar heterojunction perovskite solar cells with sequentially dip-coated deposited perovskite layers from a non-halide aqueous lead precursor. *RSC Adv.* **2020**, *10*, 5454–5461. [CrossRef]

144. Adnan, M.; Irshad, Z.; Lee, J.K. Facile all-dip-coating deposition of highly efficient $(CH_3)_3NPbI_{3-x}Cl_x$ perovskite materials from aqueous non-halide lead precursor. *RSC Adv.* **2020**, *10*, 29010–29017. [CrossRef]
145. Di Girolamo, D.; Dini, D. Electrodeposition as a Versatile Preparative Tool for Perovskite Photovoltaics: Aspects of Metallization and Selective Contacts/Active Layer Formation. *Sol. RRL* **2022**, *6*, 2100993. [CrossRef]
146. Al Katrib, M.; Perrin, L.; Planes, E. A Way to Reach 10% Efficiency with Carbon-Based Electrodeposited Mixed Perovskite Solar Cells. *Sol. RRL* **2022**, *6*, 2200777. [CrossRef]
147. Chen, C.; Chen, J.; Han, H.; Chao, L.; Hu, J.; Niu, T.; Dong, H.; Yang, S.; Xia, Y.; Chen, Y.; et al. Perovskite solar cells based on screen-printed thin films. *Nature* **2022**, *612*, 266–271. [CrossRef] [PubMed]
148. Zuo, C.T.; Scully, A.; Yak, D.; Tan, W.L.; Jiao, X.C.; McNeill, C.R.; Angmo, D.C.; Ding, L.M.; Gao, M. Self-Assembled 2D Perovskite Layers for Efficient Printable Solar Cells. *Adv. Energy Mater.* **2019**, *9*, 1803258. [CrossRef]
149. Li, Z.H.; Li, P.W.; Chen, G.S.; Cheng, Y.J.; Pi, X.D.; Yu, X.G.; Yang, D.R.; Han, L.Y.; Zhang, Y.Q.; Song, Y.L. Ink Engineering of Inkjet Printing Perovskite. *ACS Appl. Mater. Interfaces* **2020**, *12*, 39082–39091. [CrossRef]
150. Giuliano, G.; Bonasera, A.; Scopelliti, M.; Martino, D.C.; Fiore, T.; Pignataro, B. Boosting the Performance of One-Step Solution-Processed Perovskite Solar Cells Using a Natural Monoterpene Alcohol as a Green Solvent Additive. *ACS Appl. Electron. Mater.* **2021**, *3*, 1813–1825. [CrossRef]
151. Kadhim, M.J.; Mohammed, M.K.A. Fabrication of efficient triple-cation perovskite solar cells employing ethyl acetate as an environmental-friendly solvent additive. *Mater. Res. Bull.* **2023**, *158*, 112047. [CrossRef]
152. Cao, X.; Hao, L.; Liu, Z.; Su, G.; He, X.; Zeng, Q.; Wei, J. All green solvent engineering of organic-inorganic hybrid perovskite layer for high-performance solar cells. *Chem. Eng. J.* **2022**, *437*, 135458. [CrossRef]
153. Zhu, Z.; Shang, J.; Tang, G.; Wang, Z.; Cui, X.; Jin, J.; Zhou, Y.; Zhang, X.; Zhang, D.; Liu, X.; et al. Vertical distribution of PbI_2 nanosheets for robust air-processed perovskite solar cells. *Chem. Eng. J.* **2023**, *454*, 140163. [CrossRef]
154. Taylor, A.D.; Sun, Q.; Goetz, K.P.; An, Q.; Schramm, T.; Hofstetter, Y.; Litterst, M.; Paulus, F.; Vaynzof, Y. A general approach to high-efficiency perovskite solar cells by any antisolvent. *Nat. Commun.* **2021**, *12*, 1878. [CrossRef]
155. Sin, J.; Kim, H.; Kim, M.; Kim, M.; Shin, J.; Hong, J.; Yang, J. Anti-solvent treatment time approach to high efficiency perovskite solar cells with temperature of coating environmental. *Sol. Energy Mater. Sol. Cells* **2023**, *250*, 112054. [CrossRef]
156. Wang, L.; Liu, G.; Xi, X.; Yang, G.; Hu, L.; Zhu, B.; He, Y.; Liu, Y.; Qian, H.; Zhang, S.; et al. Annealing Engineering in the Growth of Perovskite Grains. *Crystals* **2022**, *12*, 894. [CrossRef]
157. Xu, W.J.; Daunis, T.B.; Piper, R.T.; Hsu, J.W.P. Effects of Photonic Curing Processing Conditions on $MAPbI_{(3)}$ Film Properties and Solar Cell Performance. *ACS Appl. Energy Mater.* **2020**, *3*, 8636–8645. [CrossRef]
158. Chen, Q.; Ma, T.T.; Wang, F.F.; Liu, Y.; Liu, S.Z.; Wang, J.A.; Cheng, Z.C.; Chang, Q.; Yang, R.; Huang, W.C.; et al. Rapid Microwave-Annealing Process of Hybrid Perovskites to Eliminate Miscellaneous Phase for High Performance Photovoltaics. *Adv. Sci.* **2020**, *7*, 2000480. [CrossRef]
159. Serafini, P.; Boix, P.P.; Barea, E.M.; Edvinson, T.; Sanchez, S.; Mora-Sero, I. Photonic Processing of $MAPbI_3$ Films by Flash Annealing and Rapid Growth for High-Performance Perovskite Solar Cells. *Sol. RRL* **2022**, *6*, 2200641. [CrossRef]
160. Turgut, S.B.; Gultekin, B. Improving power conversion efficiency by Light-Assisted annealing of triple cation perovskite layer in solar cell applications. *Sol. Energy* **2022**, *234*, 1–8. [CrossRef]
161. Li, S.N.; Ren, H.; Yan, Y. Boosting efficiency of planar heterojunction perovskite solar cells to 21.2% by a facile two-step deposition strategy. *Appl. Surf. Sci.* **2019**, *484*, 1191–1197. [CrossRef]
162. Li, S.N.; Ma, R.X.; Zhao, X.; Guo, J.H.; Zhang, Y.C.; Wang, C.C.; Ren, H.; Yan, Y. Enhanced photovoltaic performance and stability of planar perovskite solar cells by introducing dithizone. *Sol. Energy Mater. Sol. Cells* **2020**, *206*, 110290. [CrossRef]
163. Luan, F.; Li, H.; Gong, S.; Chen, X.; Shou, C.; Wu, Z.; Xie, H.; Yang, S. Precursor engineering for efficient and stable perovskite solar cells. *Nanotechnology* **2023**, *34*, 055402. [CrossRef] [PubMed]
164. Jiao, X.; Gu, W.-M.; Xu, Y.; Jiang, K.-J.; Yu, G.; Zhang, Q.-W.; Gao, C.-Y.; Liu, C.-M.; Fan, X.-H.; Yang, L.-M.; et al. Anion-exchange assisted sequential deposition for stable and efficient FAPbI3-based perovskite solar cells. *Chem. Eng. J.* **2023**, *452*, 139326. [CrossRef]
165. Bi, J.; Chang, J.; Lei, M.; Zhang, W.; Meng, F.; Wang, G. Thiourea-Assisted Facile Fabrication of High-Quality $CsPbBr_3$ Perovskite Films for High-Performance Solar Cells. *ACS Appl. Mater. Interfaces* **2023**, *14*, 48888–48896. [CrossRef] [PubMed]
166. Zhi, L.L.; Li, Y.Q.; Cao, X.B.; Li, Y.H.; Cui, X.; Ci, L.J.; Wei, J.Q. Dissolution and recrystallization of perovskite induced by N-methyl-2-pyrrolidone in a closed steam annealing method. *J. Energy Chem.* **2019**, *30*, 78–83. [CrossRef]
167. Cheng, N.; Yu, Z.; Li, W.; Lei, B.; Zi, W.; Xiao, Z.; Zhao, Z.; Zong, P.-A. A modified two-step sequential spin-coating method for perovskite solar cells using CsI containing organic salts in mixed ethanol/methanol solvent. *Sol. Energy Mater. Sol. Cells* **2023**, *250*, 112107. [CrossRef]
168. Chang, C.C.; Zou, X.P.; Cheng, J.; Ling, T.; Yao, Y.J.; Chen, D. Influence of Solution Deposition Process on Modulating Majority Charge Carrier Type and Quality of Perovskite Thin Films for Solar Cells. *Materials* **2019**, *12*, 2494. [CrossRef]
169. Liu, J.; Wang, M.; Cai, W.; Cai, R.; Shi, Y.; Bian, J. Root cause for the difference in photovoltaic parameters of perovskite solar cells prepared by one- and two-step processes. *Appl. Phys. Lett.* **2022**, *121*, 263902. [CrossRef]
170. Fong, P.W.K.; Li, G. The Challenge of Ambient Air-Processed Organometallic Halide Perovskite: Technology Transfer from Spin Coating to Meniscus Blade Coating of Perovskite Thin Films. *Front. Mater.* **2021**, *8*, 635224. [CrossRef]

171. Wang, D.; Zheng, J.M.; Wang, X.Z.; Gao, J.S.; Kong, W.G.; Cheng, C.; Xu, B.M. Improvement on the performance of perovskite solar cells by doctor-blade coating under ambient condition with hole-transporting material optimization. *J. Energy Chem.* **2019**, *38*, 207–213. [CrossRef]
172. Lee, K.M.; Lai, C.H.; Chu, W.C.; Chan, S.H.; Suryanarayanan, V. Thermal assisted blade coating methylammonium lead iodide films with non-toxic solvent precursors for efficient perovskite solar cells and sub-module. *Sol. Energy* **2020**, *204*, 337–345. [CrossRef]
173. Yu, Z.; Tao, J.; Shen, J.; Jia, Z.; Zhong, H.; Yin, S.; Liu, X.; Liu, M.; Fu, G.; Yang, S.; et al. Back-Contact Ionic Compound Engineering Boosting the Efficiency and Stability of Blade-Coated Perovskite Solar Cells. *ACS Appl. Mater. Interfaces* **2022**, *14*, 34040–34048. [CrossRef]
174. Zendehdel, M.; Nia, N.Y.; Paci, B.; Generosi, A.; Di Carlo, A. Zero-Waste Scalable Blade-Spin Coating as Universal Approach for Layer-by-Layer Deposition of 3D/2D Perovskite Films in High-Efficiency Perovskite Solar Modules. *Sol. RRL* **2022**, *6*, 2100637. [CrossRef]
175. Vijayan, A.; Johansson, M.B.; Svanstrom, S.; Cappel, U.B.; Rensmo, H.; Boschloo, G. Simple Method for Efficient Slot-Die Coating of $MAPbI_{(3)}$ Perovskite Thin Films in Ambient Air Conditions. *ACS Appl. Energy Mater.* **2020**, *3*, 4331–4337. [CrossRef] [PubMed]
176. Huang, S.H.; Guan, C.K.; Lee, P.H.; Huang, H.C.; Li, C.F.; Huang, Y.C.; Su, W.F. Toward All Slot-Die Fabricated High Efficiency Large Area Perovskite Solar Cell Using Rapid Near Infrared Heating in Ambient Air. *Adv. Energy Mater.* **2020**, *10*, 2001567. [CrossRef]
177. Bernard, S.; Jutteau, S.; Mejaouri, S.; Cacovich, S.; Zimmermann, I.; Yaiche, A.; Gbegnon, S.; Loisnard, D.; Collin, S.; Duchatelet, A.; et al. One-Step Slot-Die Coating Deposition of Wide-Bandgap Perovskite Absorber for Highly Efficient Solar Cells. *Sol. RRL* **2021**, *5*, 2100391. [CrossRef]
178. Bisconti, F.; Giuri, A.; Marra, G.; Savoini, A.; Fumo, P.; Marrazzo, R.; Zanardi, S.; Corso, G.; Po, R.; Biagini, P.; et al. Polymer-Assisted Single-Step Slot-Die Coating of Flexible Perovskite Solar Cells at Mild Temperature from Dimethyl Sulfoxide. *ChemPlusChem* **2021**, *86*, 1442–1450. [CrossRef]
179. Li, J.; Dagar, J.; Shargaieva, O.; Flatken, M.A.; Kobler, H.; Fenske, M.; Schultz, C.; Stegemann, B.; Just, J.; Tobbens, D.M.; et al. 20.8% Slot-Die Coated $MAPbI_3$ Perovskite Solar Cells by Optimal DMSO-Content and Age of 2-ME Based Precursor Inks. *Adv. Energy Mater.* **2021**, *11*, 2003460. [CrossRef]
180. Vaynzof, Y. The Future of Perovskite Photovoltaics-Thermal Evaporation or Solution Processing? *Adv. Energy Mater.* **2020**, *10*, 2003073. [CrossRef]
181. Choi, Y.; Koo, D.; Jeong, M.; Jeong, G.; Lee, J.; Lee, B.; Choi, K.J.; Yang, C.; Park, H. Toward All-Vacuum-Processable Perovskite Solar Cells with High Efficiency, Stability, and Scalability Enabled by Fluorinated Spiro-OMeTAD through Thermal Evaporation. *Sol. RRL* **2021**, *5*, 2100415. [CrossRef]
182. Becker, P.; Márquez, J.A.; Just, J.; Al-Ashouri, A.; Hages, C.; Hempel, H.; Jošt, M.; Albrecht, S.; Frahm, R.; Unold, T. Low Temperature Synthesis of Stable γ-$CsPbI_3$ Perovskite Layers for Solar Cells Obtained by High Throughput Experimentation. *Adv. Energy Mater.* **2019**, *9*, 1900555. [CrossRef]
183. Li, X.; Lin, D.X.; Chen, Z.P.; Li, Z.; Wang, J.M.; Chen, J.; Gong, L.; Xu, J.B.; Chen, K.; Liu, P.Y.; et al. Structural Regulation for Highly Efficient and Stable Perovskite Solar Cells via Mixed-Vapor Deposition. *ACS Appl. Energy Mater.* **2020**, *3*, 6544–6551. [CrossRef]
184. Lohmann, K.B.; Patel, J.B.; Rothmann, M.U.; Xia, C.Q.; Oliver, R.D.J.; Herz, L.M.; Snaith, H.J.; Johnston, M.B. Control over Crystal Size in Vapor Deposited Metal-Halide Perovskite Films. *ACS Energy Lett.* **2020**, *5*, 710–717. [CrossRef] [PubMed]
185. Qiu, L.B.; He, S.S.; Liu, Z.H.; Ono, L.K.; Son, D.Y.; Liu, Y.Q.; Tong, G.Q.; Qi, Y.B. Rapid hybrid chemical vapor deposition for efficient and hysteresis-free perovskite solar modules with an operation lifetime exceeding 800 hours. *J. Mater. Chem. A* **2020**, *8*, 23404–23412. [CrossRef]
186. Qiu, L.; He, S.; Jiang, Y.; Qi, Y. Metal halide perovskite solar cells by modified chemical vapor deposition. *J. Mater. Chem. A* **2021**, *9*, 22759–22780. [CrossRef]
187. Tumen-Ulzii, G.; Matsushima, T.; Adachi, C. Mini-Review on Efficiency and Stability of Perovskite Solar Cells with Spiro-OMeTAD Hole Transport Layer: Recent Progress and Perspectives. *Energy Fuels* **2021**, *35*, 18915–18927. [CrossRef]
188. Shen, Y.; Deng, K.; Li, L. Spiro-OMeTAD-Based Hole Transport Layer Engineering toward Stable Perovskite Solar Cells. *Small Methods* **2022**, *6*, 2200757. [CrossRef]
189. Niu, X.X.; Li, N.X.; Zhu, C.; Liu, L.; Zhao, Y.Z.; Ge, Y.; Chen, Y.H.; Xu, Z.Q.; Lu, Y.; Sui, M.L.; et al. Temporal and spatial pinhole constraints in small-molecule hole transport layers for stable and efficient perovskite photovoltaics. *J. Mater. Chem. A* **2019**, *7*, 7338–7346. [CrossRef]
190. Zhou, X.S.; Qiu, L.L.; Fan, R.Q.; Wang, A.N.; Ye, H.X.; Tian, C.H.; Hao, S.; Yang, Y.L. Metal-Organic Framework-Derived N-Rich Porous Carbon as an Auxiliary Additive of Hole Transport Layers for Highly Efficient and Long-Term Stable Perovskite Solar Cells. *Sol. RRL* **2020**, *4*, 1900380. [CrossRef]
191. Du, Q.; Shen, Z.T.; Chen, C.; Li, F.M.; Jin, M.Q.; Li, H.L.; Dong, C.; Zheng, J.H.; Ji, M.X.; Wang, M.T. Spiro-OMeTAD:Sb_2S_3 Hole Transport Layer with Triple Functions of Overcoming Lithium Salt Aggregation, Long-Term High Conductivity, and Defect Passivation for Perovskite Solar Cells. *Sol. RRL* **2021**, *5*, 2100622. [CrossRef]
192. Cao, W.; Zhang, J.; Lin, K.; Qiu, L.; Li, J.; Dong, Y.; Xia, D.; Yang, Y. Redox engineering of spiro-OMeTAD based hole transport layer enabled by ultrathin Co(III)-grafted carbon nitride nanosheets for stable perovskite solar cells. *Nano Energy* **2022**, *104*, 107924. [CrossRef]

193. Liu, J.; Dong, Q.S.; Wang, M.H.; Ma, H.R.; Pei, M.Z.; Bian, J.M.; Shi, Y.T. Efficient Planar Perovskite Solar Cells with Carbon Quantum Dot-Modified spiro-MeOTAD as a Composite Hole Transport Layer. *ACS Appl. Mater. Interfaces* **2021**, *13*, 56265–56272. [CrossRef] [PubMed]
194. Ye, X.Q.; Yu, P.W.; Shen, W.Q.; Hu, S.F.; Akasaka, T.; Lu, X. Er@C-82 as a Bifunctional Additive to the Spiro-OMeTAD Hole Transport Layer for Improving Performance and Stability of Perovskite Solar Cells. *Sol. RRL* **2021**, *5*, 2100463. [CrossRef]
195. Lou, Q.; Lou, G.; Guo, H.; Sun, T.; Wang, C.; Chai, G.; Chen, X.; Yang, G.; Guo, Y.; Zhou, H. Enhanced Efficiency and Stability of n-i-p Perovskite Solar Cells by Incorporation of Fluorinated Graphene in the Spiro-OMeTAD Hole Transport Layer. *Adv. Energy Mater.* **2022**, *12*, 2201344. [CrossRef]
196. Zheng, J.; Li, F.; Chen, C.; Du, Q.; Jin, M.; Li, H.; Ji, M.; Shen, Z. Perovskite Solar Cells Employing a $PbSO_4(PbO)_4$ Quantum Dot-Doped Spiro-OMeTAD Hole Transport Layer with an Efficiency over 22%. *ACS Appl. Mater. Interfaces* **2022**, *14*, 2989–2999. [CrossRef]
197. Zheng, X.; Wang, H.; Ye, F.; Chen, C.; Ke, W.; Zhang, W.; He, C.; Tai, Y.; Fang, G. Organic-inorganic hybrid hole transport layers with SnS doping boost the performance of perovskite solar cells. *J. Energy Chem.* **2022**, *68*, 637–645. [CrossRef]
198. Han, W.; Ren, G.; Liu, J.; Li, Z.; Bao, H.; Liu, C.; Guo, W. Recent Progress of Inverted Perovskite Solar Cells with a Modified PEDOT:PSS Hole Transport Layer. *ACS Appl. Mater. Interfaces* **2020**, *12*, 49297–49322. [CrossRef]
199. Elbohy, H.; Bahrami, B.; Mabrouk, S.; Reza, K.M.; Gurung, A.; Pathak, R.; Liang, M.; Qiao, Q.Q.; Zhu, K. Tuning Hole Transport Layer Using Urea for High-Performance Perovskite Solar Cells. *Adv. Funct. Mater.* **2019**, *29*, 1806740. [CrossRef]
200. Yi, H.M.; Wang, D.; Duan, L.P.; Haque, F.; Xu, C.; Zhang, Y.; Conibeer, G.; Uddin, A. Solution-processed WO_3 and water-free PEDOT: PSS composite for hole transport layer in conventional perovskite solar cell. *Electrochim. Acta* **2019**, *319*, 349–358. [CrossRef]
201. Yang, X.; Lv, F.; Yao, Y.; Li, P.; Wu, B.; Xu, C.; Zhou, G. Boosting Performance of Inverted Perovskite Solar Cells by Diluting Hole Transport Layer. *Nanomaterials* **2022**, *12*, 3941. [CrossRef] [PubMed]
202. Hu, W.; Xu, C.Y.; Niu, L.B.; Elseman, A.M.; Wang, G.; Yan, D.; Yao, Y.Q.; Liao, L.; Zhou, G.D.; Song, Q.L. High Open-Circuit Voltage of 1.134 V for Inverted Planar Perovskite Solar Cells with Sodium Citrate-Doped PEDOT:PSS as a Hole Transport Layer. *ACS Appl. Mater. Interfaces* **2019**, *11*, 22021–22027. [CrossRef] [PubMed]
203. Redondo-Obispo, C.; Ripolles, T.S.; Cortijo-Campos, S.; Alvarez, A.L.; Climent-Pascual, E.; de Andres, A.; Coya, C. Enhanced stability and efficiency in inverted perovskite solar cells through graphene doping of PEDOT:PSS hole transport layer. *Mater. Des.* **2020**, *191*, 108237. [CrossRef]
204. Wang, Z.-J.; Li, J.-W.; Zhang, D.-Y.; Yang, G.-J.; Yu, J.-S. Improving efficiency of inverted perovskite solar cells via ethanolamine-doped PEDOT:PSS as hole transport layer. *Chin. Phys. B* **2022**, *31*, 087802. [CrossRef]
205. Xu, L.; Chen, X.; Jin, J.; Liu, W.; Dong, B.; Bai, X.; Song, H.; Reiss, P. Inverted perovskite solar cells employing doped NiO hole transport layers: A review. *Nano Energy* **2019**, *63*, 103860. [CrossRef]
206. Lee, P.H.; Li, B.T.; Lee, C.F.; Huang, Z.H.; Huang, Y.C.; Su, W.F. High-efficiency perovskite solar cell using cobalt doped nickel oxide hole transport layer fabricated by NIR process. *Sol. Energy Mater. Sol. Cells* **2020**, *208*, 110352. [CrossRef]
207. Chen, M.J.; Qiao, H.W.; Zhou, Z.R.; Ge, B.; He, J.J.; Yang, S.; Hou, Y.; Yang, H.G. Homogeneous doping of entire perovskite solar cells via alkali cation diffusion from the hole transport layer. *J. Mater. Chem. A* **2021**, *9*, 9266–9271. [CrossRef]
208. Choi, F.P.G.; Alishah, H.M.; Gunes, S. Cerium and zinc co-doped nickel oxide hole transport layers for gamma-butyrolactone based ambient air fabrication of $CH_{(3)}NH_{(3)}PbI_3$ perovskite solar cells. *Appl. Surf. Sci.* **2021**, *563*, 150249. [CrossRef]
209. Syafiq, U.; Ataollahi, N.; Scardi, P. Progress in CZTS as hole transport layer in perovskite solar cell. *Sol. Energy* **2020**, *196*, 399–408. [CrossRef]
210. Cheng, N.; Liu, Z.; Li, W.; Yu, Z.; Lei, B.; Zi, W.; Xiao, Z.; Sun, S.; Zhao, Z.; Zong, P.-A. Cu_2ZnGeS_4 as a novel hole transport material for carbon-based perovskite solar cells with power conversion efficiency above 18%. *Chem. Eng. J.* **2023**, *454*, 140146. [CrossRef]
211. Liang, J.-W.; Firdaus, Y.; Azmi, R.; Faber, H.; Kaltsas, D.; Kang, C.H.; Nugraha, M.I.; Yengel, E.; Ng, T.K.; De Wolf, S.; et al. Cl_2-Doped CuSCN Hole Transport Layer for Organic and Perovskite Solar Cells with Improved Stability. *ACS Energy Lett.* **2022**, *7*, 3139–3148. [CrossRef]
212. Kim, G.; Kwon, N.; Lee, D.; Kim, M.; Kim, M.; Lee, Y.; Kim, W.; Hyeon, D.; Kim, B.; Jeong, M.S.; et al. Methylammonium Compensation Effects in MAPbI(3) Perovskite Solar Cells for High-Quality Inorganic CuSCN Hole Transport Layers. *ACS Appl. Mater. Interfaces* **2022**, *14*, 5203–5210. [CrossRef] [PubMed]
213. Perumbalathodi, N.; Su, T.-S.; Wei, T.-C. Antisolvent Treatment on Wet Solution-Processed CuSCN Hole Transport Layer Enables Efficient and Stable Perovskite Solar Cells. *Adv. Mater. Interfaces* **2022**, *9*, 2201191. [CrossRef]
214. Zhang, J.J.; Zhu, S.; Gao, C.; Gao, C.X.; Liu, X.Z. Low Temperature Producing Copper-Doped Gallium Oxide as Hole Transport Layers of Perovskite Solar Cells Enhanced by Impurity Levels. *Sol. RRL* **2022**, *6*, 2100861. [CrossRef]
215. Li, G.-R.; Gao, X.-P. Low-Cost Counter-Electrode Materials for Dye-Sensitized and Perovskite Solar Cells. *Adv. Mater.* **2020**, *32*, 1806478. [CrossRef]
216. Lyu, B.; Yang, L.; Luo, Y.; Zhang, X.; Zhang, J. Counter electrodes for perovskite solar cells: Materials, interfaces and device stability. *J. Mater. Chem. C* **2022**, *10*, 10775–10798. [CrossRef]
217. Xu, C.; Zhao, X.; Ma, J.; Guo, J.; Ma, T.; Wu, M. Recent Progresses in Carbon Counter Electrode Materials for Perovskite Solar Cells and Modules. *ChemElectroChem* **2021**, *8*, 4396–4411. [CrossRef]

218. Lee, J.W.; Jeon, I.; Lin, H.S.; Seo, S.; Han, T.H.; Anisimov, A.; Kauppinen, E.I.; Matsuo, Y.; Maruyama, S.; Yang, Y. Vapor-Assisted Ex-Situ Doping of Carbon Nanotube toward Efficient and Stable Perovskite Solar Cells. *Nano Lett.* **2019**, *19*, 2223–2230. [CrossRef]
219. Hughes, D.; Meroni, S.M.P.; Barbe, J.; Raptis, D.; Lee, H.K.H.; Heasman, K.C.; Lang, F.; Watson, T.M.; Tsoi, W.C. Proton Radiation Hardness of Perovskite Solar Cells Utilizing a Mesoporous Carbon Electrode. *Energy Technol.* **2021**, *9*, 2100928. [CrossRef]
220. Zhao, X.; Xu, C.; Wang, X.; Guo, J.; Wu, M. Construction of multilevel network structured carbon nanofiber counter electrode and back interface engineering in all inorganic HTL-free perovskite solar cells. *Colloids Surf. A* **2022**, *648*, 129420. [CrossRef]
221. Sepalage, G.A.; Weerasinghe, H.; Rai, N.; Duffy, N.W.; Raga, S.R.; Hora, Y.; Gao, M.; Vak, D.; Chesman, A.S.R.; Bach, U.; et al. Can Laminated Carbon Challenge Gold? Toward Universal, Scalable, and Low-Cost Carbon Electrodes for Perovskite Solar Cells. *Adv. Mater. Technol.* **2022**, *7*, 2101148. [CrossRef]
222. Guo, M.; Wei, C.Y.; Liu, C.C.; Zhang, K.; Su, H.J.; Xie, K.Y.; Zhai, P.; Zhang, J.; Liu, L. Composite electrode based on single-atom Ni doped graphene for planar carbon-based perovskite solar cells. *Mater. Des.* **2021**, *209*, 109972. [CrossRef]
223. Forgacs, D.; Wojciechowski, K.; Malinkiewicz, O. *High-Efficient Low-Cost Photovoltaics: Recent Developments*; Petrova-Koch, V., Hezel, R., Goetzberger, A., Eds.; Springer International Publishing: Cham, Germany, 2020; pp. 219–255. [CrossRef]